

THROMBOLITIC STROMATOLITES OF THE CAMBRIAN GALLATIN  
FORMATION: SIGNIFICANCE OF WELL-PRESERVED DOPPELGANGERS

A Thesis submitted to the faculty of  
San Francisco State University  
In partial fulfillment of  
the requirements for  
the Degree

Master of Science

In

Geoscience

by

Sonicah Sanon

San Francisco, California

May 2020

Copyright by

Sonicah Sanon

2020

CERTIFICATION OF APPROVAL

I certify that I have read THROMBOLITIC STROMATOLITES OF THE CAMBRIAN GALLATIN FORMATION: SIGNIFICANCE OF WELL PRESERVED DOPPELGANGERS by Sonicah Sanon, and that in my opinion this work meets the criteria for approving a thesis submitted in partial fulfillment of the requirement for the degree Master of Science in Geoscience: Paleobiology at San Francisco State University.



---

Yadira Ibarra, Ph.D.

Assistant Professor



---

Mary Leech, Ph.D.

Professor



---

John Caskey, Ph.D.

Associate Professor

# THROMBOLITIC STROMATOLITES OF THE CAMBRIAN GALLATIN FORMATION: SIGNIFICANCE OF WELL PRESERVED DOPPLEGANGERS

Sonicah Sanon

San Francisco, California

2020

## ABSTRACT

Microbialites constitute some of the earliest records of life on Earth, but diagenetic processes often blur or erase a clear signal of the depositional accretionary processes that control their morphological intricacies. This study examines the role of sedimentation, metazoan skeletal clasts, and depositional environment on the accretion of well-preserved stromatolitic-thrombolitic microbialites from the Upper Cambrian Gallatin Formation of western Wyoming collected from the eastern flank of Rendezvous mountain. Microbialites exhibit dome shaped decimeter-scale columns that occur as part of shallowing upward parasequences deposited during the late Cambrian marine transgression recorded throughout the Cordilleran of Laurentia.

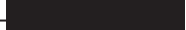
Data derived from thin section point counts, clast size to depositional angle comparisons, and chromatic mesosequencing (CMS) suggests: i) coarse-grained agglutinated textures are not restricted to modern day microbialites, ii) ancient microbialites were not restricted to biologically exclusive environments. The presence of trace fossils, ooid clasts and complete fossil segments within micritic microfacies suggests metazoan bioturbation, proximal fossil origin, or in situ necrolysis. The presence of allochthonous clasts in precipitated microspar and micrite suggests an active integration of the grains by microbial mat communities. Evidence of biogenicity includes the incorporation of very fine to medium sand sized grains at high angles as well as the presence of *Girvanella*, and *Renalcis* in micrite and microsparitic laminae. The textural details provided herein suggest coarse-grained microbialites may be more

common in the Paleozoic than previously thought and has important implications for using recent insights into modern coarse-grained microbialites to interpret the paleoecology and taphonomy of microbialites from the early Paleozoic.

I certify that the Abstract is a correct representation of the content of this thesis.



\_\_\_\_\_  
Chair, Thesis Committee

\_\_\_\_\_

Date

## ACKNOWLEDGEMENTS

I would like to thank Dr. Yadira Ibarra for her contributions as well as her guidance and patience. Without her this project would not be possible. I am grateful for my editors and good friends, Fatima T. Johura and Jose R. Ruiz who have helped take this project and turn it into something beautiful. Also my sisters, Gabriella Sanon, Nadege and Hermanie Motley who offered solace and made me laugh when this project drove me to tears. I would like to thank my parents, Sonie L. Sanon, Joseph and Patricia Sanon for supporting me whenever I came to them. Lastly, a special thanks to my partner and friend Thibault Monnier whose encouragement kept my faith in my work alive.

## TABLE OF CONTENTS

List of Tables .....	ix
List of Figures .....	x
List of Appendices .....	xii
1.0 Introduction.....	1
2.0 Geologic Setting and Previous Work.....	4
2.1 Cambro-Ordovician Geology and Paleoenvironment of Present-day Rendezvous Mountain, Wyoming .....	4
2.2 Gros Ventre Limestone (Middle Cambrian) .....	5
2.3 Gallatin Limestone (Upper Cambrian) .....	6
2.4 Bighorn Dolomite (Middle-Upper Ordovician).....	7
3.0 Methods and Approach.....	8
3.1 Bighorn Dolomite (Middle-Upper Ordovician).....	8
3.2 Petrographic Preparation and Imaging.....	8
3.3 Point Counting and Clast Size Analysis .....	9
3.4 CMS (Chromatic Mesosequencing) Analysis .....	10
3.5 Statistical Analysis .....	11
4.0 Results.....	12
4.1 Field observations .....	12
4.2 Mesostructural Observations .....	13
4.3 Microstructural Observations.....	14

4.4 Point count results.....	16
4.5 CMS results.....	17
4.6 Ooid diameter and angle height .....	20
4.7 Statistical analysis of point count data.....	20
4.8 Statistical analysis of CMS data .....	20
5.0 Discussion.....	21
5.1 Qualitative data interpretation.....	21
5.1.1 Stratigraphic interpretation .....	21
5.1.2 Mesostructural and microstructural interpretation.....	25
5.2 Quantitative data interpretation.....	25
5.2.1 Point count and lamination angle-ooid diameter .....	25
5.2.2 CMS of STC 1 .....	26
5.2.3 CMS and quantitative analysis interpretation of STC 2 .....	28
6.0 Conclusions.....	29
Reference .....	31
Appendices.....	64

## LIST OF TABLES

Table	Page
1. Point Count Data.....	59
2. STC Point Count Data.....	61
3. Spearman's Correlation Data .....	62
4. Ooid Grain Diameter to Lamina Height Angle Comparisons.....	63

## LIST OF FIGURES

Figures	Page
1. Geologic range of microbialite textures.....	33
2. Location of Rendezvous Mountain section.....	34
3. Field photo of site.....	35
4. Stratigraphic, lithologic, and petrographic summary of the study.....	36
5. Ooid grain diameter and angle height comparison.....	37
6. CMS analysis of STC1.....	38
7. CMS analysis of STC2.....	39
8. Stromatolite lenses of the Gallatin Formation.....	40
9. Representative outcrop photographs and corresponding lithologic section.....	41
10. Outcrop photographs of STC microbialite facies.....	42
11. Mesostructure of STC microbialites.....	43
12. Fossils and clasts within the Gallatin Formation.....	44
13. Microbialites within sample STC1.....	45
14. Microstructure of microbialite sample STC1.....	46
15. Microstructure of microbialite sample STC1.....	47
16. Truncation of microbially precipitated fabric.....	48
17. Point count data of layer STC.....	49
18. Microfacies frequency models.....	50
19. Texture variability in STC 1.....	51
20. The variability of allochem content in STC 1.....	52
21. Microfacies frequency models of STC 2.....	53
22. Texture variability in STC 2.....	54
23. The variability of allochem content in STC 1.....	55

24. Relationship between clast (oid) size and lamination angle.....	56
25. Stratigraphic column and depositional model of Rendezvous section.....	57
26. Textural similarities found in modern and ancient microbialites.....	58

## LIST OF APPENDICES

Appendix	Page
1. Raw data of STC 1 microfacies frequency per strip.....	64
2. Raw data of STC 1 microfacies and texture frequency per module.....	65
3. Raw data of STC 2 microfacies frequency per strip.....	66
4. Raw data of STC 2 microfacies and texture frequency per module.....	67
5. Descriptive Statistics and Histogram of Average Fossil Content.....	68

## 1.0 INTRODUCTION

Microbialites are organosedimentary deposits that accrete as a result of trapping and binding and/or mineral precipitation associated with a benthic microbial community (Burne & Moore, 1987). Three common microbialite mesofabric (cm-scale fabrics, *sensu* Shapiro, 2000) have been described: stromatolites (laminated), thrombolites (clotted), and dendrolites (branching clusters) (Riding, 2011). Of the three common microbialite forms, fine-grained stromatolites have the longest geological record originating in the Late Archean (~3.5 Ga) and becoming more ubiquitous throughout the late Precambrian-Proterozoic (Awramik, 1988) (Figure 1). However, despite their classification as microbialites, most ancient stromatolites do not contain clear evidence of microbial mediation and most stromatolites lack microfossils—a likely result of diagenetic alteration that can obscure or erase a clear signal of biogenicity (Grotzinger & Knoll, 1999). For this reason, it is important to investigate the potential extrinsic (e.g., environmental) and intrinsic (e.g., microbial communities, local sedimentation, etc.) factors that control stromatolite accretion and their diagenesis through time and in different depositional environments. Being able to determine depositional versus diagenetic controls on stromatolite textures is critical to discern their potential as paleoenvironmental and/or evolutionary indicators in the geologic record (Grotzinger and Knoll, 1999).

Stromatolites were prevalent in the Precambrian, where they reached peak levels in the Paleoproterozoic, and began to decline in the Neoproterozoic and into the

Proterozoic-Paleozoic transition (Awramik & Sprinkle, 1999). The advent of the Cambrian Period's species radiation, when life gave rise to complex fauna was considered a potential mechanism for stromatolite decline (Fischer 1965; Garrett 1970; Pratt, 1982), but was later viewed as problematic because stromatolite decline started before the appearance of metazoans (Awramik & Sprinkle, 1999). The metazoan exclusion hypothesis suggested that metazoans may have burrowed and bioeroded microbial mat bodies, competed for shallow ocean floor area, and reduced the availability of dissolved calcium carbonate in ancient oceans (Garrett, 1970; Planavsky and Ginsburg, 2009; Pratt, 1982). The reason for stromatolite decline after their prevalence in the Precambrian remains poorly understood, but other hypotheses exist (Riding, 2000, 2006). Furthermore, at approximately the same time as the Cambrian Explosion, microbialites exhibited a shift in internal patterning (mesofabric) and external morphology (mesostructure), a possible form of adaptation to new threats and changes in their environment (Garrett 1970; Hoffman, 1976; Horodyski, 1977). During the early Cambrian, stromatolites became sparse giving rise to thrombolites—unlaminated-clotted cryptalgal structures (Aitken, 1967; Riding, 2011) that are present in marine settings today (Figure 1).

The late Cambrian of western Wyoming contains extensive stromatolitic microbialites (Lochman & Hu, 1960; Saltzman, 1999) whose textures may hold clues to the environmental influences that resulted in the subsequent continued decline of stromatolites in marine environments in the Phanerozoic. In this study, depositional, textural, and ecological relationship of a microbialite unit from the Upper Cambrian Gallatin Formation of western Wyoming are investigated. The objectives of this research

were to examine three common Phanerozoic marine stromatolite assumptions. One of the assumptions is that stromatolites become increasingly rare in subtidal marine environments. Indeed, previous research suggests that the stromatolites described herein formed in a lagoon with restricted seawater circulation (Martin et al., 1980). Another assumption is that the advent of animals and their activities (e.g., burrowing) contributed to the decline in stromatolite abundance, thus rendering the co-occurrence of stromatolites and metazoans an anachronistic phenomenon (Garrett, 1970). Finally, most studies of Phanerozoic stromatolites have shown that fine grained fabrics that were common in the Precambrian, become rare in the Phanerozoic (Riding, 2011). For example, modern microbialites are coarse-grained (Feldmann & Mckenzie, 1998; Logan, 1961; Reid et al., 2000) and the oldest known stromatolites that incorporate allochthonous clasts during accretion are from the Late Devonian (Suarez-Gonzalez et al., 2019). The paucity of ancient examples of coarse-grained microbialites limits our ability to explore and understand how ancient microbial biofilms interacted with allochthonous sedimentation in shallow marine settings and apply knowledge of observations from modern marine microbialites.

To address biofilm-sedimentation relationships and stromatolite accretion mechanisms, this thesis describes the depositional and macro- to micro textural features of Upper Cambrian marine stromatolitic microbialites that accreted via an iterative balance of authochthonous micrite and ooid mud sedimentation along the shallow shores of Laurentia in present day western Wyoming.

## 2.0 GEOLOGIC SETTING AND PREVIOUS WORK

### 2.1 *Cambro-Ordovician Geology and Paleoenvironment of Present-day Rendezvous Mountain, Wyoming*

The stratigraphy of the Teton Range is comprised of sandstone, shale, variable beds of limestone as well as dolomite (Figure 3). The Cambrian Gros Ventre Formation and Gallatin Limestone contain sub-units of shales and limestones that measure an average of 200 meters in thickness (USGS, 1988). In the Teton and Gros Ventre Ranges the Gallatin Formation measures approximately 55 m in thickness. The Park Shale member of the Gros Ventre measures approximately 67 m in the Teton Range (Blackwelder, 1913; Miller, 1936). Sedimentary strata of the Gallatin Formation generally thin westward where the combined thickness of the Open-Door and the DuNoir Members measure approximately 25 m in the Teton Range (Miller, 1913).

The Gros Ventre and Gallatin Formations contain evidence of two shallowing upward successions containing sequence divisions deposited in intrashelf basins, subtidal sand shoals, and intertidal zones (Martin et al., 1980, Saltzman, 1998). The first shallowing upward sequence occurs near the top of the Park Shale Member at the appearance of flat pebble conglomerate and the second shallowing upward sequence occurs at the top of the Gallatin Formation, preceding the unconformity with the overlying Bighorn Dolomite. Increased sedimentation rates in a shallow-water carbonate factory is attributed to the regressive character of the sequences, not necessarily to a drop in sea level (Martin et al., 1980).

Overlying the Cambrian strata is the Ordovician Bighorn Dolomite with an erosional unconformity at the base and uppermost contacts (Figure 4A). The Bighorn

Dolomite is characterized by massive-bedded deposits of dolomitic mottlestones indicating deposition in a shallow subtidal setting. The Bighorn Dolomite measures approximately 46 to 90 m in the Teton Range (Blackwelder, 1913).

### ***2.2 Gros Ventre Limestone (Middle Cambrian)***

The Gros Ventre Formation is divided into members, according to Martin et al. (1980). The Wolsey Shale Member occurs first, overlain by the Death Canyon Member and then the Park Shale Member. It is suspected that the Park Shale Member is the oldest layer sampled in the section measured for this project, but the underlying sequences will be briefly described as a formality.

The Wolsey Shale Member is a ledge-forming unit of fine-grained quartz sandstone subunits interbedded with micaceous shale; in the uppermost portion micaceous clay is eroded leaving glauconitic calcite-cemented quartz arenite (Martin et al., 1980). The Wolsey Shale Member contains mostly greenish-gray soft micaceous shales approximately 30.5 m in thickness, the lower portion of the member contains sandstones that increase in thickness eastward, while the upper layers contain calcareous sandstone and argillaceous limestone with numerous tubular markings, which possibly represent borings, shales have weathered into a steep slope covered by talus debris from overlying limestone layers (Miller, 1963). The Death Canyon Member is marked by micritic-microsparitic lithology (Martin et al., 1980) consisting of fine grained, dark grey and black limestone mottled with brown. The member possesses a thickness of about 87 m within the Teton range and displays a prominent escarpment (Miller, 1963).

The Park Shale Member is approximately 67 m in thickness (Miller, 1963) contains more micritic-microsparitic and variable bedding than the underlying units. The

petrology of the lower portion of the member is characterized by green-grey shale, at times purplish to dark green due to the presence of hematite as well as glauconite with recurring lenses of micaceous quartz sandstone (Miller, 1963, Martin et al., 1980). The green shale-sublitharenite pattern indicates deposition in an intrashelf basin. Sedimentary structures of this division include desiccation cracks, small scale ripple or wrinkle structures and burrows (Miller, 1963; Martin et al., 1980). The middle sequence of the Park Shale Member consists of alternating beds of cryptalgal laminites, ripple-bedded micrites, and flat pebble conglomerates deposited on more elevated portions of tidal flats (Martin et al., 1980). Lastly, the petrology of the upper portion of the member is characterized by a majority of lime mud intraclasts, fossil fragments (trilobite, brachiopod, bivalve, and echinoderm fragments), ooids, peloids, glauconite, quartz silt, and dolomite rhombs.

### ***2.3 Gallatin Limestone (Upper Cambrian)***

The Gallatin Limestone is comparatively more fossiliferous than the underlying and overlying units (Martin et al, 1980). The Gallatin Formation is subdivided into two members, the DuNoir Member and overlying the Open Door Member. The Gallatin Formation is followed by an unconformity at the contact with the Bighorn Dolomite (Martin et al., 1980). The DuNoir Member contains abundant intraclasts, fossils, ooids, quartz sand and silt and is characterized by massive dark gray mottled limestone with yellowish-brown limonite. The numeration of fossil and allochem content was done by Martin et al. (1980) in which echinoderm and trilobite fragments are the most abundant fossils, followed by brachiopod fragments, algal rods, and some discontinuous stromatolites. There are prominent fossiliferous shale and quartz sand facies within the

DuNoir Member that are interpreted to have formed during shoaling upwards events on intertidal and supratidal flats. The ooid facies of the DuNoir Member were deposited during small transgressive episodes within shallow carbonate platform shoals (Martin et al., 1980).

The Open-Door Member is described by Miller (1963) as the Middle Shaley and Upper Limestone Divisions measuring approximately 25 to 27 m within the Teton Range. The Open Door Member contains burrowed and bioturbated limestones with mottled textures formed by iron-oxide or limonite stained burrows, stylolites and areas of recrystallization (Martin et al., 1980). There are abundant ooids, some of which display complete neomorphism, a large amount of them are deformed (Martin et al., 1980). The occurrence of ooid facies marks the middle of the Open Door Member (Saltzman, 1999). Above the oolitic layer are unbranching stromatolitic columns with calcitic and dolomitized layers with an axial plane (domical shape produces a pseudo-axis) (Martin et al., 1980). The Open Door Member contains rippled and finely laminated sediments, ooids and fossils indicative of shallow subtidal setting. It is a prograding sequence accumulated in low energy epeiric carbonate platforms surrounded by lime mud shoals where wave action is generated by wind. These continental beaches were situated upon what is now the Wyoming craton, not unlike the modern carbonate shelves of the Bahamas (Martin et al., 1980).

#### ***2.4 Bighorn Dolomite (Middle-Upper Ordovician)***

The Bighorn Dolomite is a prominent cliff-forming unit of mottled and massive dolomite limestone. Fossiliferous constituents include trilobite, brachiopod and mollusk fragments (Blackwelder, 1913; Holland & Patzkowsky, 2012). The depositional setting is

interpreted to be an open marine shallow subtidal setting but also contains restricted marine shallow subtidal, laminated peritidal facies, and deep subtidal mudstones (Holland & Patzkowsky, 2012).

### 3.0 METHODS AND APPROACH

#### *3.1 Outcrop Description and Sample Collection*

The section examined in this study is located in Grand Teton National Park, Wyoming along the Cirque Trail on the eastern flank of Rendezvous Range (Figures 2-3). The Park Shale Member of the Gros Ventre Formation is poorly exposed, composed of platy shale debris, with intermittent layers of sandstone and flat pebble conglomerate. Overlying the Gros Ventre Formation, the Gallatin Limestone Formation was measured. Bed thicknesses ranged from 10 cm to beds greater than 3 m in thickness. The Gallatin Formation's contact with the overlying Bighorn Dolomite was not accessible due to the steepness of the cliff outcrop. The Bighorn Dolomite is estimated to have a thickness greater than 10 m at the study site. Rock samples varying from 15 cm to approximately 30 cm in diameter were collected from massive beds at approximately every meter of the section (see Figure 4C). Some samples displayed superficial bioturbation, fossil impressions, and signs of chemical weathering. Images of the site and hand samples were captured using a Canon PowerShot SX530.

#### *3.2 Petrographic Preparation and Imaging*

Laboratory analyses entailed cutting and polishing rock samples to examine the mesofabric (i.e., cm-scale) appearance. Over one hundred thin sections were created, thirteen of which were prepared by Wagner Petrographic. Scanned images of the rock

slabs were taken using an EPSON high resolution scanner. Petrographic images were captured using Zeiss Axio imager.M2m petrographic microscope coupled with an Axiocam 506 color camera. Photomosaic imagery was accomplished using the Zeiss Zen Pro Software to capture the sample microfacies (i.e., sub-mm scale) and facilitate the counting of stromatolite laminae. Microstructural, petrographic, and optical analyses were carried out to examine the microfacies within the mineral matrix, reveal evidence of microfossils, and document any potential diagenetic processes.

### ***3.3 Point Counting and Clast Size Analysis***

Point counting analyses was accomplished with FIJI (Fiji Is Just ImageJ) using the Cell Counter plugin software with a grid overlay where each unit area ranged between 300 to 2,000 mm<sup>2</sup>, depending on grain size. A grid size averaging fifteen by twenty units was overlain on several samples from each sampled layer. Three or more grids were used for standard thin sections (four or more for large format thin sections) to ensure a representative point count comparison, except for layers that are uniform and bereft of fossils (green shales or sandstone) for which one grid was created. For each grid, a total of three-hundred points were counted to avert sampling bias (a standard amount according to Flugel (2004). Each point was allocated to a constituent category (e.g., bryozoan, echinoid, ooid, etc.). The categories are listed in Table 1. A total of over thirteen-thousand points were accounted for in the sum of the analyses.

To understand the grain size distribution of clasts within the microbialite samples, allochthonous grains were measured along with corresponding angles of deposition within sample STC 1. The angular degree of the lamination that ooids occur on or within were first measured and saved using FIJI's angle measurement tool. The diameters of

grains deposited on lamina were measured following their respective angles using the line tool (Figure 5). Twenty-five grains were measured on a total of thirty-five different lamination angles on sample STC 1, totaling over eight-hundred clast measurements.

### ***3.4 CMS (Chromatic Mesosequencing) Analysis***

Although point counting provides the frequency of constituents, it does not allow for the observations of a temporal relationship between the occurrence of microbial lamina and skeletal fragments. To address the temporal relationship of allochems and mesofabric, a new approach to analyzing organosedimentary structures was utilized, which is referred to here as chromatic mesosequencing (CMS).

The development of CMS focuses on the transformation of temporal visual data into categories and the creation of color-generalized areas to represent these categories (e.g., micrite and microspar). A scaled, scanned image or petrographic image of the sample is divided into twenty-four 0.05 mm vertical *strips* for sample STC 1 and forty-four for sample STC 2 (Figures 6B and 7A) using the FIJI Montage to Stack and Make Montage features. Throughout each strip, corresponding areas of micrite or microspar matrix microfacies are represented by a band of color, in turn creating an image of recurring bands of various lengths. The quantified microfacies frequency bands per strip were used to produce an approximate mound profile.

Lamination exclusion, a process in which complete lamina are counted based on two conditions: (i) frequency bands are of similar or justifiable size (i.e., a significantly larger band sits between two sister bands of similar size), and (ii) sister bands traverse the sample across three or more strips. This process allows omission of clots, a fabric routinely found offsetting lamina in thrombolitic-stromatolitic mounds.

Vertical divisions of the column facilitate microfacies categorization and provide an understanding of how microfacies vary across the column, but possess inherent caveats including the inability to represent temporal relationship.

Horizontal divisions moving upward in the column—termed *modules*, allow the frequency bands created to fall into a designated area for comparison of allochems and microfacies through time. STC 1 was divided into ten modules and STC 2 was divided into five modules, each module is approximately 20 mm long containing a fourteen by seven point-count grid. The numeration of frequency bands and laminae were correlated with fossil and clast population.

The creation of simplified images through CMS prevents misinterpretation of inferences from the visual data. In the case of this project, the microfacies frequency and laminations quantified are unmistakable based on a CMS image. CMS data that is coupled with allochem point count data (described in section 3.3), allows for clearer insight into the spatiotemporal relationship between the laminations and the allochems (including skeletal fossil content). Samples STC1 and STC 2 were analyzed in this study, but it should be noted that STC 1 possesses a full bodied mesosequence, providing an optimal evaluation in comparison to STC 2.

### ***3.5 Statistical analysis***

Models and data output tables were generated using IBM SPSS 24 and Excel. Point count data was analyzed using raw value and mean comparison to understand the role of fossil abundance and clast size in how microfacies change through time. Preliminary normality tests were run to decide if parametric correlation tests (Pearson's  $r$ ) or nonparametric correlation tests (Spearman's  $\rho$ ) were appropriate. Correlation tests

were used to determine whether the explanatory variables possess a strong association. Correlation scatter plot overlays were used to display covariance between variables and deposition. The magnitude of  $R^2$ , whether suggesting a strong or weak correlation would be neither problematic nor preferred because the variables involved are unpredictable.

## 4.0 RESULTS

### *4.1 Field observations*

The northeastern flank of Rendezvous mountain is a limestone-shale sequence that rests upon Precambrian layered metagabbro and laminated sandstone substrata (Figure 4A). The beds within the Rendezvous range dip 25 degrees to the southwest (Love et al., 1992). Local faults cut through the cliff face of the Gallatin Formation. The Cambrian Gros Ventre Formation is poorly exposed, covered in talus and debris from overlying units but is suspected to measure over 30 m. Near the base of the section, platy unfossiliferous green shales of the Park Shale Member create a gentle slope.

The Gallatin Limestone is a cliff forming sequence (Figure 3) overlying the Gros Ventre Formation marked by the initial appearance of closely spaced packstones and flat pebble conglomerate beds that alternate with laminated mudstone (Figure 4B). The bedding is variable but recurrent. The upper DuNoir Member is characterized by layers of flat pebble conglomerate facies that create coarsening upward parasequences with laminated carbonate mudstones (Figure 4B). Carbonate mudstone beds contain lenses of fossiliferous mottled limestones and massive packstones measuring a total 4 m. Overlying the DuNoir Member is the Open Door Member, distinguishable by the initial appearance of a thick green carbonate mudstone and isolated lenticular stromatolite

lenses (Figure 8). Facies of the Open Door Member are predominately composed of massive limonite-mottled wackestone that form coarsening upward parasequences with oolitic/oncolitic packstone/grainstone facies. Beds that exhibit ooid-oncolitic and fossiliferous facies are shown in Figures 9C-D. Stromatolitic microbialites (~14 cm thick beds) with unbranching columns occur near the top of the section within massive mottled limestone (Figure 9B and Figure 10). Parabolic pseudolamina are pronounced on the column surface denoted by deep striations etched into a weathered surface (Figure 10). Above the microbialite unit is a thick layer of richly fossiliferous mottled limestone and chert (Figure 4B and 9B) with notable bioturbation visible in hand sample ('U' samples in Figure 4C). An erosional unconformity occurs at the topmost layers where the cliff face is truncated.

Following the unconformity is the Bighorn Dolomite Formation (Figure 4B and 9A). As described by Blackwelder (1913), the weathered surface of the Bighorn Dolomite exhibits raised welts and branching depressions.

#### ***4.2 Mesostrucutural Observations***

Mesostructural observations of the microbialites were performed on scanned images taken from the 'STC' layer (Figures 4C and 11). The polished slabs reveal rhythmic lamination offset or truncated by allochems. The lamina is often hard to distinguish as patterns are incomplete or poorly defined. Despite this, the images present two fundamental observations (i) there are three distinguishable microfacies: ooid-rich layers that are darker in color, light-grey sediment with no noticeable clasts or fossil content, and iron-rich sediment (limonite) possessing an ochre-brown tone, and (ii) continuous laminations within the column are no more than 0.40 mm in thickness.

### ***4.3 Microstructural Observations***

The microfacies of the Gros Ventre Formation's Park Shale Member is composed of primarily chlorite, limonite, and ferrous fossils impressions. The upper arenitic portions exhibit common sandstone composition of quartz, muscovite and biotite. Laminations visible in hand sample are recognizable in thin section, where darker bands contain greater amounts of limonite. Wrinkle structures appear to be surficial as runnels do not extend beyond 0.3mm.

The DuNoir Member of the Gallatin Formation is composed of green carbonate mudstones, flat pebble conglomerates, packstones and mottled limestones (Figure 4E). Laminated mudstone samples exhibit uniformly distributed glauconite with sparse muscovite and biotite. Networks of sparitic burrows are present as well are grains of ferrous oxides, possibly siderite or hematite (Figure 4E). Flat pebble conglomerates have compositions identical to that of the laminated mudstone, primarily the pebbles showing high glauconitic content and lamination, which may have been fragments of previously deposited mudstone layers. The surrounding ground mass contains less glauconite, instead peloids, trilobite fragments and sparitic burrows are the main textures. The mottled limestones are fine grained with no glauconite present, large recrystallized burrows within a micritic and iron rich matrix.

The Open Door Member contains packstones, fossiliferous mottled limestones, oncolitic-oolitic grainstones and microbialite columns (Figure 4E, Table 1 Sample ID prefixes STL-U). Packstones contain small intraclasts and pebbles, rip-up clasts and small amounts of glauconite (Figure 4E). The mottled limestones of this subunit are similar in description to previous layers, composed of a fine grained calcitic matrix with

prominent limonite staining in areas of recrystallization. Burrows and stylolites are common while skeletal fragments were not, a majority of which appeared to be broken (layers H and U in Figure 4B). In the middle of the Open Door Member is a layer composed of oncolitic-oolitic facies that contains burrows that are ~1.5 mm in diameter and large pebble-sized clasts within a micritic matrix (Layer L in Figure 4C). There are numerous monaxial spicules (Figure 12C) throughout most of the Gallatin Formation, characteristic of the form genus *Gallatinospongia* described by Okulitch and Bell (1955). The occurrence of *Gallatinospongia* indicates a biozone attributed to the Upper Cambrian (Okulitch and Bell 1955). Sponges of the Cambrian are composed of calcium carbonate but possess morphologic similarities to hexactinellid sponges (Harvey, 2010). There are abundant hexaclinal triaxon spicules identifiable with hexactinellid sponges (Figure 12B)

Microbialites occur at the base and upper portion of the Open Door Member. The uppermost occurrence of thrombolitic stromatolite columns resemble the genus form *Colonnella*, or at times *Conophyton*-like in shape (conical axes are significantly offset, some laminations appear truncated or reflexed) (Figure 10). Fossils of several calcimicrobes were evident, predominately *Renalcis* and *Girvanella* (Figure 12D and 13).

The textural features of microbialite sample STC1 are shown in Figure 14. Key attributes of the microbialite microfacies include micritic dendritic features that alternate with microspar layers (Figure 14A-B), spar-occluded fenestrae (Figure 14B), skeletal and ooid clasts (Figure 14C), and *Girvanella* microfossils (Figure 14E). Figure 15A highlights alternating micrite and microspar laminae shown in cross polarized light. Figures 15 B-E denote allochthonous clasts embedded in micrite at a high angle, where the outer portion of the grain is encrusted by the microfossil *Girvanella*. Figure 16 shows

the influence of skeletal fossils on the microbialite textures, whereby trilobite thoracic fragments and other allochthonous clasts influence the shape of the micritic and microsparitic layers of the microbialite (Figure 16A-B).

#### ***4.4 Point count results***

Percent composition of each bed are averaged between beds of similar petrography based on point count data from Table 1. The laminated green mudstones of the DuNoir Member were entirely unfossiliferous composed of 78% micrite, 16% glauconite, 6% siderite. Flat pebble conglomerates were also unfossiliferous comprised of 57% large clasts, 26% peloids, 12% micrite and less than 4% sparite, siderite and burrows. Mottled limestones of the DuNoir Member contain 73% micrite, 16% limonite stained fill, 8% burrows and less than 6% sparite and bivalves.

Mottled limestones vary little throughout the Gallatin Formation with each bed with a 73.5% micrite and 12.5% limonitic micrite composition, also 9% fossiliferous consisting of 8.5% burrows and less than 1% bivalve fragments. Tempestites are composed of an average of 22.5% sparite, 21% clasts, 20% micrite, 18.5% rip-up clasts, 8% ooids and peloids and 3% stylolites. The layer of oolitic facies consists of primarily of 44% oncoids and ooids, 26% peloids, fossil content is 3% trilobite fragments and 1% porifera spicules. The uppermost portion of the Gallatin Formation above the calcimicrobial bed contains variable layers averaging 28% fossil content (15% burrows, 9% trilobite, 4% bivalve fragments, 1% ooid) and 72% non-fossil content (15% pelsparite, 10% biomicrite, 9% pelmicrite, 6% micrite, 4% peloid, 1% glauconite).

The first stromatolitic lens bed (Figure 8) within Open Door Member 3% fossiliferous excluding calcimicrobial fossils, 8.3% microbial, 80% micrite, 7% limonite,

6% burrow or occluded fenestrae, 3% sparite, 2% diagenetic textures, and less than 3% trilobite and porifera spicules. The stromatolitic microbialite bed (STC) bed is composed of micrite (47%) and microspar (15%) (Table 2 Sample ID STL, Figure 17A and B). Similar to the previous microbial bed it contains 3% bioclasts and 8.3% calcimicrobial impressions making it approximately 87% unfossiliferous. The remaining composition is 17.5% clasts, 4.3% dolomite and stylolites, and 5.3% fenestrae. The mean number of clasts in micrite is substantially greater, nearly five times more than the amount of clasts found in microspar. (Figure 17B).

The average fossil content of each layer increases with time, the highest being the uppermost mottled limestone layer (28%) and the lowest being the green laminated mudstone and flat pebble conglomerate layers (0-1%).

#### ***4.5 CMS results***

The mean total of microfacies frequency bands per strip for STC 1 is 38.8; the maximum reaching 63 counts with the minimum being 44 (Figure 18A, Appendix 1). The scatter plot produces a slight bimodal trend that bubbles nearing strips five and six as well as twelve and thirteen. The trend of micrite and microspar frequency from strips one to fourteen mimics the total trend, bulging upwards on either side of strips eight through ten. In theory this would be closer to the center of the microbialite column if the laminae were not clotted and followed a pattern similar to a domical stromatolite.

The average microfacies frequency bands per module is 81.7 (Figure 18B). Modular frequency counts excluding modules one and seven, show a general increase in banding (Figure 18B). Average modular frequency counts for micrite is 40.5 and 41.2 for microspar. There is generally no variability in the amount of each microfacies within the

sample. Lamination count (the number of combined, equidimensional microfacies frequency bands) were 49 for micrite and 37 for microspar (Figure 18 C, Appendix 2).

Mean texture content per module is approximately 13.7 (Figure 19A and B). The greatest count occurs within modules two and nine and the lowest within module ten. Clasts are the most frequent textures within the sample, primarily in modules two and eight while its minimum value occurs in module ten. Fenestrae, diagenetic textures, and bioclasts were relatively close in value between the averages of 3.3 and 2.0. Fenestrae frequency reaches a maximum in module two and a minimum in module one. Diagenetic textures and bioclast follow a similar fluctuating trend peaking near modules two, four, or five and again in module eight for bioclasts. The relatively lowest occurrences are within modules one, six, nine for diagenetic texture and ten for bioclasts. Put simply, all textures show an increase in module two after which fenestrae and diagenetic textures follow polar trends whilst bioclasts and clasts follow a similar movement except for module four. The values contributing to this trend include both bioclast and clast allochem types found within micrite and microspar microfacies. This required further examination as described below.

Clast and bioclasts occur within micrite and microspar, the difference in population of both allochem types in either microfacies (micrite or microspar) appeared significant (Figure 20A and B, Appendix 2). The average frequency of clasts within micrite is 9.1 as opposed to clasts in microspar found to be approximately 2.6. Moreover, the average frequency of bioclasts in micrite and microspar are 1.4 and 0.6, respectively. This shows that overall, allochems occur more frequently in micrite than microspar.

STC 2 yields a standard total of 20.0 frequency bands per strip, with a maximum microfacies frequency of 36 and a minimum of 9 (Figure 21A, Appendix 3). The plot produced a parabolic trend that heightens nearing strips twenty-two to twenty-nine, closest to the center of a column (Figure 21A). The average micrite and microspar frequency per strip is 10.0 with a maximum of 18 and a minimum of 4. Both follow a nearly identical trend though micrite shows slightly more variance in raw data values.

The mean number of frequency bands per module is 165.2 (Figure 21B). The trend of modular frequency bands generally increases, the further up the column the higher the number of microfacies frequency bands. There is little variability between microfacies, the average frequency band counts for micrite and microspar are 82.0 and 83.2, respectively. The lamination count of micritic microfacies is 7.6 and microspar is 9.2 (Figure 21C).

Average texture content per module was 40.4 (Figure 22A) The highest amount of 55 occurs within module one and the lowest value of 24 within module three. Clasts were again the most frequent textures within the sample returned a value of 31.4 followed by fenestrae (23.6), bioclasts (9.0), and diagenetic textures (8.4). Because STC 2 contained evidence of the *Renalcis*, a category reserved for *microbial* occurrences was created. Microbial textures were found to have a mean frequency of 12.2 per module, the maximum count occurs in module five, the same module in which the lowest frequency of diagenetic textures occurs.

Based on scatter plots created (Figure 22B) it is apparent that there is no pronounced relationship between textures except an inverse trend among bioclasts and diagenetic textures and a more harmonious trend between microbial textures and clasts.

The polarity between bioclasts and diagenetic textures is most obvious in module four where both reach their highest magnitude. Microbial textures and clasts dip within module three while displaying a general rise on either side of it. Mean frequency of clasts within micrite is 23.4 as opposed to clasts in microspar found to be approximately 8.0. The standard frequency of bioclasts in micrite was found to be 7.4 and microspar 1.6 (Figure 23A and B). Similar to sample STC 1, overall STC 2 displays that allochems occur more frequently in micrite than microspar.

#### ***4.6 Ooid diameter and angle height***

Scatter plots based on lamina angle and ooid diameter are shown in Figure 24A. Ooids of larger diameter are deposited at high and low angles, but overall, more ooids were found at lower angles (Figure 24B, Table 4).

#### ***4.7 Statistical analysis of point count data***

Based on descriptive statistical summaries of the point count data, the mean fossil content of the section is 34 fossils with a minimum and maximum values of 0 and 84 respectively (Appendix 5A). The results derived from the Shapiro-Wilk normality test reveals that the distribution of fossil content within the section is not normal and is skewed to the right (Appendix 5B). Seventy percent of samples lie within a range of zero to forty-five fossil frequency while thirty percent occur within a range of forty-five to one hundred.

#### ***4.8 Statistical analysis of CMS data***

Due to case values less than twenty-five it is assumed the distribution is not normal therefore a nonparametric correlation test was used. The correlation coefficients yielded from Spearman's  $\rho$  show predominately weak to nonexistent correlations with

poor statistical significance from STC 1 data (Table 3A). Exceptions include an inverse correlation between clasts and the frequency of micritic bands (-0.606) with a significance level less than 0.05 while clasts in microspar showed a statistically insignificant and relatively weak positive correlation (0.222). Bioclasts within micrite and microspar produced a strong negative relationship with  $R^2$  values of -0.328 and -0.497. This result was unexpected as the most clast present within the column occur within micrite not microspar. Moderate and insignificant inverse correlations appear between diagenetic textures with in both micrite and microspar (-0.390 and -0.351 respectively).

Strong to very strong correlations exist from STC 2 correlation (Table 3B), most notably between the abundance of microbial fossils within microspar, the amount of bioclasts in microspar ( $R^2$  values of 0.900 and -0.894 respectively) as well as the occurrence of fenestrae in micrite (0.700) all of which were significant. Moderate correlations occur between microbial fossils and micrite (0.500), bioclasts in micrite (-0.410), clasts within micrite (0.359) but all values are insignificant. Additional moderate correlations exist between diagenetic textures and microspar (-0.462) and clasts and microspar (-0.308).

## 5.0 DISCUSSION

### ***5.1 Qualitative data interpretation***

#### *5.1.1 Stratigraphic and depositional setting interpretation*

According to the stratigraphy of the measured section, a single shoaling upwards sequence within the Open Door Member of the Gallatin Formation is apparent. The inaccessibility of previous layers and the eroded surfaces following the fossiliferous unit

of variable bedding (UG) creates some uncertainty in how the sequence progresses.

Based on the exposed strata two deepening events can be inferred.

The cyclical pattern of glauconitic mudstone with intermittent sandstone and flat pebble conglomerate preceding the Open Door Member (Table 1 Sample ID prefixes AA-E) and the appearance of the overlying flat pebble conglomerate facies, indicates that deposition began in relatively deep water (intrashelf basin). The glauconite-rich pebbles found within the conglomerate contain facies identical to the previous shale layer. Based on these observations, it is assumed that strong currents removed, transported and redeposited partially lithified shales offshore (Myrow et al., 2004) (Figure 25 ). Fine-grained micaceous arenites like those found in the Park Shale Member are habitually deposited in slow moving or standing water such as deltaic or lagoonal-carbonate platform settings. The lack of burrowing within green shales and the flat pebble conglomerates of the Gros Ventre Formation's lower sequence indicates an anoxic setting which prevented chemical alteration of siderite and pyrite. Glauconite grains within the shales are not coated indicating little physical transportation, commonly found in deeper water settings. The presence of peloids and burrows within upper Gros Ventre Formation's flat pebble conglomerate matrices suggests the initial interaction of metazoans with deposited sediment. The stromatolitic lenses (Figure 8) that occur at the base of Open Door Member indicate sediment aggradation in shallow water within the photic zone.

Packstones containing numerous shallow water fossils often precede thick layers of highly burrowed mottled limestones displaying a coarsening upward pattern. The high abundance of spar and rip up clasts within the packstone/grainstone facies suggests a high

energy environment (Figure 4E). Rip-up clasts contain fossils and large coated grains formed by the removal of material from previously deposited limestone, later to be reincorporated into the sequence. Point count data express the variability in fossil and ooid content within packstones to be relatively high (Table 1 Sample ID prefixes G, K and L). This may be a result of the increase in fossil availability through time. As ocean floor space becomes more populated, more skeletal remains are deposited, removed and redeposited. Mottled limestones also exhibit a high range in ooid and fossil fragment population and may owe this outcome to conditions similar to packstones. Varicolored limestone of the Open Door Member indicate the presence of siderite and pyrite derived limonite primarily due to exposure (increased oxidation and hydration from bioturbation).

The transition from packstone limestone facies into calicimicrobial-rich biomicrite within the section indicates regressive character. It is speculated to be due to the aggradation of sediment and not sea level rise. Based on stratigraphy it is understood that microbial bioherms are situated in the fore-reef zone bordering ooid shoals (Figure 25B). This is unlike the conventional perception of ancient microbialites being restricted to quiescent lagoonal environments and unable to proliferate in otherwise erratic conditions.

A majority of ooid grains in the overlying oolite layer are large and well sorted suggesting prolonged mobilization in high energy followed by gradual decrease in velocity. Thrombolitic stromatolites that occur within the fossiliferous mottled limestones of the Open Door Member precede the high energy oolite-oncolite facies and contain smaller ooid grains than the oolite layer. These thrombolitic stromatolites are likely lateral equivalents of the thrombolitic boundstones described by Saltzman (1999).

The small sand-sized ooids found within these calcimicrobial columns are suspected to occur due to transportation of saltating grains from shallow water shoal environments further seaward toward flanking microbial colonies (Figure 25). As the agitation in the environment diminishes, large gravel sized ooids are deposited first while smaller ooids and clasts are distally deposited and captured by microbial filaments. Coarse-grained sediment capture may stem from not only increased suspension time but also selective entrainment capacity. Perhaps the transportation energy involved was sufficient enough to convey grains of variable sizes but the adhesion capacity of extracellular polymeric substances (EPS) secreted by microbial colonies was capable of selectively capturing ooids 300  $\mu\text{m}$  in diameter or less. This would explain the presence of ooids as well as the appearance of *Renalcis* in previous packstone/grainstone facies (Figure 4B and C, Layer 'K', Figure 12D).

The presence of unfractured trilobite hooks and thoracic fragments indicates proximal origin within a subtidal marine setting characteristic of a carbonate platform (Flügel, 2004, Moutinho et al., 2016) and not lagoonal as previously understood (Martin, 1980). Within the lower portion of STC 1 an unfragmented thoracic segment lies parallel to deposition, thereby truncating and diverting precipitated microfacies (Figure 16A). Ooid-rich mud is deposited followed by the eventual overgrowth of a microbial mat thus capping off further mud deposits. This anomaly cannot be explained by abiotic processes such as *lift-off* (disruption and tearing of microbial mats by currents) and is supporting evidence of biogenicity. A similar case is seen in STC 2, cranidium and thoracic fragments obstruct the growth of calcimicrobial mats creating a clast-rich micritic gap (Figure 16B).

### *5.1.2 Mesostructural and microstructural interpretation*

Thrombolitic-stromatolite beds exhibit a change in matrix material, shifting from fine mud to fossiliferous ooid mud. This translates to a shallow water-carbonate platform setting transitioning to ooid sand bars—a consequence of aggradation (Figure 25).

Lenticular microbialites within the first bed (STL) are less than 4 cm in height and columnar microbialites within the second bed (STC) reach a height of over 14 cm. A difference between short and more elongate structures may be grain size. Reduced grain size requires a larger amount of sediment to create full-bodied columns as opposed to coarse grains (e.g. ooid, sand and fossil fragments). Fossil origin of these layers differ in that the surrounding facies of the first microbial bed possesses syndimentary fossils. This means ocean floor space was being shared with other species. The basis of this is the presence of several trilobite bodies seen in hand sample and several closely arranged echinoid spines (Figure 12B). Further evidence includes the discontinuity of the lenses, allotting space for potential colonization. Although, some trilobite fragments have been identified but were in very few numbers.

## **5.2 Quantitative data interpretation**

### *5.2.1 Point Count and lamination angle-oid diameter*

Analyses of ooid diameter and their associated lamination angle provide further support for the biogenicity of the STC stromatolites. Based on angle diameter comparisons, there is no robust relationship between ooid diameter and the angle of repose. Results show that irrespective of the steepness of the angle, grains approximately 300  $\mu\text{m}$  or less are being captured. A small number of sand sized grains were deposited at angles exceeding the 40° angle of repose. Grains trapped at high angles provide

suggestive evidence for microbial mat adhesion that would otherwise be less likely on an abiotic domed surface (Frantz et al., 2015). The ooid diameters recorded in this analysis are comparable to the ooid sizes found in modern marine coarse-grained stromatolitic thrombolites from the Bahamas (Feldmann & Mckenzie, 1998).

### *5.2.2 CMS of STC 1*

The CMS analysis of STC 1 shows that the number of frequency bands dip towards the center of the column creating a double peak (Figure 18A). This was not expected as the overall shape of the structure is domed (Figure 11D). A straight column with consistently oriented lamina axes and where lamination minima occur at the margins would produce a parabolic shape as is demonstrated in sample STC 2 (Figure 11E). Sample STC 1 demonstrates a bimodal trend, as the column is slightly sinuous. The axes of lamina gradually shift to either side of the pseudo-axis which is marked by the highest point of the column. The cause of the bimodal trend is uncertain but could be the result of phototactic behavior or the smothering of budding microbial mounds by incoming sediment (Figure 16A-B). The pseudo-axis of a sinuous column would be where the lowest number of laminations occur except for the margins.

The total number of frequency bands as well as laminations increase throughout the modules except for a preceding spike in module one (Figure 18B). This general upturn is due to an increased frequency in microbially induced precipitation and intermittent micritic deposition, which may indicate that during the latter portion of deposition, more frequent periods of exposure and inundation occurred. The nearly 1:1 ratio of microsparitic to micritic laminations remains constant throughout the modules.

This consistency in matrix type reveals that as time moves forward there are nearly equal amounts of carbonate precipitation and sediment deposition.

Evidence from Spearman's correlation involving microsparitic and micritic microfacies indicates robust negative correlation values between clasts and bioclasts. The relationship between the presence of micrite and the abundance of clasts and bioclasts contradicts the original apparent assumption that allochems are most frequent within micritic facies. Based on modular point count data, clasts were the most abundant textures within the sample, sharply rising and falling repeatedly (Figure 19B).

Petrographic images of STC 1 (Figure 14A-D) suggest a recurrence of allochems within micrite but point count data coupled with CMS suggests otherwise. This indicates that although allochems are commonly found within generalized areas of micrite, clasts and fossil fragments are not evenly disbursed throughout areas of micrite. Examination of clast in micrite and micrite point count data show that the number of clasts within micrite are approximately half the frequency of micrite (Figure 20A-B). This population of clasts is most often located toward the base of micritic lamina (Figure 14D) and even more so within lamina toward the base of the column. Near the top of the column the number of clasts become sparse as the number of micrite frequency bands increase thus creating a strong negative correlation. The undulating frequency of clasts within micrite may be attributed to periodic episodes of storm activity creating microscale fining upward sequences. Diagenetic textures follow a nearly identical trend to clast with a moderate correlation, partly due to the susceptibility of ooid grains to dolomitization.

The amount of allochems, primarily bioclasts, residing in microspar are scarce corroborating the concept that filamentous calcimicrobes are not incorporating notable

amounts of clasts in areas of precipitation. This does not disprove the notion that burrowing and large sediment grains are affecting the structure of microbial columns in general. Instead clasts and skeletal content rest above or around microsparitic laminations but seldomly lie within it.

### *5.2.3 CMS and quantitative analysis interpretation of STC 2*

The primary understanding derived from the band frequency per strip is the column produces a parabolic plot consistent with a domical mound (Figure 21A). A parabolic shape insinuates a majority of the mound is undisturbed or is in the beginning stages of growth. In the case of a presumably fragmented or short-lived sequence, the ratio of micrite to microspar is nearly 1:1. The modular frequency of microfacies generally increases with time, similar to STC 1 this denotes an increase in precipitation and deposition. Examination of laminations indicate a general increase in microsparitic lamina while micrite displays a nearly constant amount excluding a dip in module three (Figure 21C). Considering both cases, the amount of microspar lamina increases as the deposition of micrite decreases, a potential indication that a prolonged period of mat growth.

A strong positive correlation between microspar and microbial fossils coupled with the positive relationship between fenestrae and micrite supports the idea that spar-occluded fenestrae are the results gases emitted through metabolic processes and decomposition (Table 3A). Microsparitic lamina are microbially precipitated followed by the deposition of mud and the formation of gas bubbles. This is where postsedimentary biologic interaction occurring within the column becomes most visible. Generalized areas of microsparite show a robust negative correlation with bioclast content, further

validating the concept that areas of precipitation are not incorporating large amounts of skeletal fragments.

## 6.0 CONCLUSIONS

This study examines the role of sedimentation, metazoan skeletal clasts, and depositional environment on the accretion of well-preserved stromatolitic-thrombolitic microbialites from the Upper Cambrian Gallatin Formation of western Wyoming collected from the eastern flank of Rendezvous mountain. Evidence of stromatolite biogenicity include: (i) the presence of irregular fenestrae parallel to laminar fabric ii) the impediment of growth by laterally deposited skeletal fragments, and (iii) the presence of coarse-grained clasts at high angles, which can only be achieved through adhesion.

Thrombolitic- stromatolites accrete by integrating sediment and fossils to (i) build upward while precipitating calcite or (ii) these components obstruct growth but are not detrimental to the column. The incorporation of coarse-grained clasts ( $>200\mu\text{m}$ ) within organosedimentary structures is considered a relatively recent geologic phenomenon and mostly a characteristic restricted to stromatolites from the Cenozoic. The textural details provided herein suggest coarse-grained microbialites may be more common in the Paleozoic than previously thought and has important implications for using recent insights into modern coarse-grained microbialites to interpret the paleoecology and taphonomy of microbialites from the early Paleozoic. Furthermore, the presence of sand-sized ooids and essentially whole trilobite segments indicates a subtidal open ocean environment amongst benthic fauna and not a lagoonal depositional setting as previously interpreted.

This study also casts doubt on the concept that metazoans have an adverse effect on microbialites given that regardless of the occurrence of bioturbation and proximal habitation, microbialite growth persists. Supporting observations include (i) the presence of unabraded trilobite thoracic segments within the stromatolite column signifying proximal origination of allochems, and (ii) the presence of burrows within micrite suggests in situ metazoan interaction.

## REFERENCES

1. Aitken, J. D. (1967). Classification and environmental significance of cryptalgal limestones and dolomites, with illustrations from the Cambrian and Ordovician of southwestern Alberta. *Journal of Sedimentary Petrology*, 37(4), 1163–1178.
2. Awramik, S. M., & Sprinkle, J. (1999). Proterozoic stromatolites: The first Marine Evolutionary Biota. *Historical Biology*, 13(4), 241–253.  
<https://doi.org/10.1080/08912969909386584>
3. Blackwelder, E. (1913). Origin of the Bighorn Dolomite of Wyoming. *Bulletin of the Geological Society of America*, 24, 607–624.
4. Burne, R. V., & Moore, L. S. (1987). Microbialites: Organosedimentary Deposits of Benthic Microbial Communities. *Palaios*, 2(3), 241. <https://doi.org/10.2307/3514674>
5. Feldmann, M., & Mckenzie, J. A. (1998). Stromatolite-Thrombolite Associations in a Modern Environment, Lee Stocking Island, Bahamas. *Palaios*, 13(2), 201–212.
6. Fischer, A. G., 1965, Fossils, early life, and atmospheric history: National Academy of Sciences Proceedings, v. 53, p. 1205-1215.
7. Flügel, Erik. *Microfacies of Carbonate Rocks: Analysis, Interpretation and Application*. Berlin ; New York: Springer, 2004. Print.
8. Frantz, C. M., Petryshyn, V. A., & Corsetti, F. A. (2015). Grain trapping by filamentous cyanobacterial and algal mats: Implications for stromatolite microfabrics through time. *Geobiology*, 13(5), 409–423. <https://doi.org/10.1111/gbi.12145>
9. Garrett, P. (1970). Phanerozoic Stromatolites : Noncompetitive Ecologic Restriction by Grazing and Burrowing Animals. *Science*, 169(3941), 171–173.
10. Grotzinger, J. P., & Knoll, A. H. (1999). STROMATOLITES IN PRECAMBRIAN CARBONATES: Evolutionary Mileposts or Environmental Dipsticks? *Annual Review of Earth and Planetary Sciences*, 27(1), 313–358.  
<https://doi.org/10.1146/annurev.earth.27.1.313>
11. Harvey, T. (2010). Carbonaceous preservation of Cambrian hexactinellid sponge spicules. *Biology Letters*, 6(6), 834-837.
12. Microflora, P., Islands, B., Significance, C. :, Author, S., & Hofmann, H. J. (1976). SEPM Society for Sedimentary Geology Paleontological Society. Source: *Journal of Paleontology*, 50(6), 1040–1073. <https://doi.org/10.2110/palo>.
13. Holland, S. M., & Patzkowsky, M. E. (2012). Sequence architecture of the Bighorn Dolomite, Wyoming , USA: Transition to the late Ordovician Icehouse. *Journal of Sedimentary Research*, 82, 599–615. <https://doi.org/10.2110/jsr.2012.52>
14. Horodyski, R. (1977). Environmental influences on columnar stromatolite branching patterns; examples from the middle Proterozoic Belt Supergroup, Glacier National Park, Montana. *Journal of Paleontology*, 51(4), 661-671.
15. Lochman, C., & Hu, C. (1960). Upper Cambrian Faunas from the Northwest Wind River Mountains, Wyoming. Part I. *Journal of Paleontology*, 34(5), 793–834.
16. Logan, B. W. . (1961). Cryptozoon and associated stromatolites from the Recent, Shark Bay, Western Australia. *Journal of Geology*, 69(5), 517–533.
17. Love, J., Weitz, J., & Hose, R. (1954). Geologic Map of Wyoming. *Science (New York, N.Y.)*, 119(3088), 327.
18. Martin, W. D., Fischer, H. J., Keogh, R. J., & Moore, K. (1980). The Petrology of Limestones in the Upper Gros Ventre and Gallatin Limestone Formations. In A. Harrison (Ed.), *Stratigraphy of Wyoming* (31st ed., pp. 37–51). Wyoming Geological Association Annual Field Conference Guidebook.
19. Mata, S.A., Harwood, C.L., Corsetti, F.A., Stork, N.J., Eilers, K., Berelson, W.M., and Spear, J.R., 2012, Influence of Gas Production and Filament Orientation on Stromatolite

- Microfabric: *Palaios*, v. 27, p. 206–219, doi:10.2110/palo.2011.p11-088r.
20. Myrow, P. M., Tice, L., Archuleta, B., Clark, B., Taylor, J. F., & Ripperdan, R. L. (2004). Flat-pebble conglomerate: Its multiple origins and relationship to metre-scale depositional cycles. *Sedimentology*, 51(5), 973–996. <https://doi.org/10.1111/j.1365-3091.2004.00657.x>
  21. Okulitch, V., & Bell, W. (1955). Gallatinospongia, a New Siliceous Sponge from the Upper Cambrian of Wyoming. *Journal of Paleontology*, 29(3), 460–461
  22. Planavsky, N., & Ginsburg, R. N. (2009). Taphonomy of Modern Marine Bahamian Microbialites. *Palaios*, 24(1), 5–17. <https://doi.org/10.2110/palo.2008.p08-001r>
  23. Pratt, B. R. (1982). Stromatolite decline - a reconsideration. *Geology*, 10(10), 512–515. [https://doi.org/10.1130/0091-7613\(1982\)10<512:SDR>2.0.CO;2](https://doi.org/10.1130/0091-7613(1982)10<512:SDR>2.0.CO;2)
  24. Reid, R. P., Visscher, P. T., Decho, A. W., Stolz, J. F., Bebout, B. M., Dupraz, C., Macintyre, I. G., Paerl, H. W., Pinckney, J. L., Prufert-Bebout, L., Steppe, T. F., & DesMarais, D. J. (2000). The role of microbes in accretion, lamination and early lithification of modern marine stromatolites. *Nature*, 406(6799), 989–992. <https://doi.org/10.1038/35023158>
  25. Riding, R. (2000). Microbial carbonates: The geological record of calcified bacterial-algal mats and biofilms. *Sedimentology*, 47(SUPPL. 1), 179–214. <https://doi.org/10.1046/j.1365-3091.2000.00003.x>
  26. Riding, R. (2006). Microbial carbonate abundance compared with fluctuations in metazoan diversity over geological time. *Sedimentary Geology*, 185(3-4 SPEC. ISS.), 229–238. <https://doi.org/10.1016/j.sedgeo.2005.12.015>
  27. Riding, R. (2011). Microbialites, stromatolites, and thrombolites. *Encyclopedia of Earth Sciences Series*, 9781402092114, 635–654. [https://doi.org/10.1007/978-1-4020-9212-1\\_196](https://doi.org/10.1007/978-1-4020-9212-1_196)
  28. Saltzman, M. R. (1999). Upper Cambrian carbonate platform evolution, Elvinia and Taenicephalus zones (pterocephaliid-ptychaspid biomere boundary), northwestern Wyoming. *Journal of Sedimentary Research*, 69(4), 926–938. <https://doi.org/10.2110/jsr.69.926>
  29. Shapiro, R. S. (2000). A Comment on the Systematic Confusion of Thrombolites. *Palaios*, 15(2), 166. <https://doi.org/10.2307/3515503>
  30. Suarez-Gonzalez, P., Benito, M. I., Quijada, I. E., Mas, R., & Campos-Soto, S. (2019). ‘Trapping and binding’: A review of the factors controlling the development of fossil agglutinated microbialites and their distribution in space and time. *Earth-Science Reviews*, 194(December 2018), 182–215. <https://doi.org/10.1016/j.earscirev.2019.05.007>

FIGURES

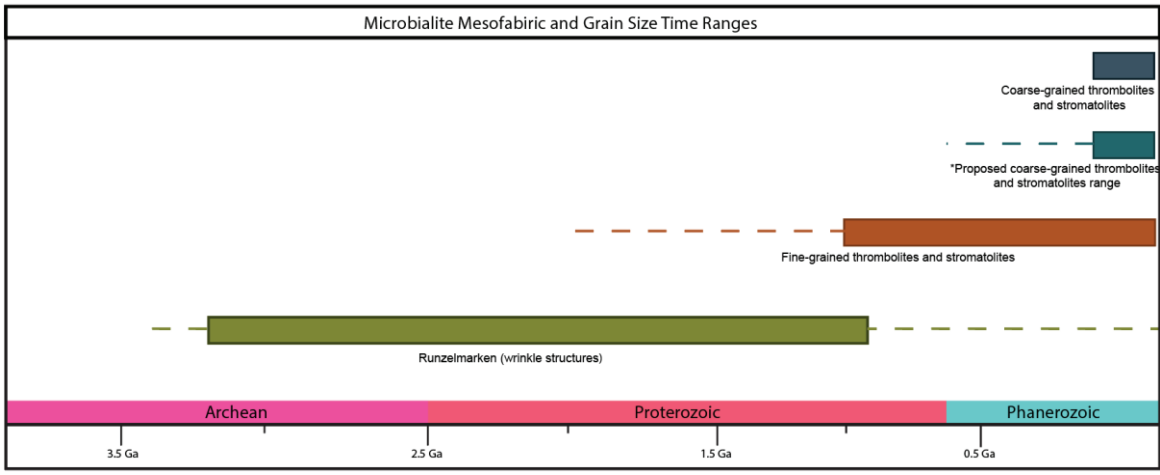


Figure 1. *Geologic range of microbialite textures.* Coarse-grained microbialites are thought to be features of the latter part of the Phanerozoic. Evidence from this work suggests that coarse-grained microbialites occur during the middle to late Cambrian, indicating that speculated occurrences (marked by dashed lines) should extend into the early Phanerozoic (after Riding, 2011).

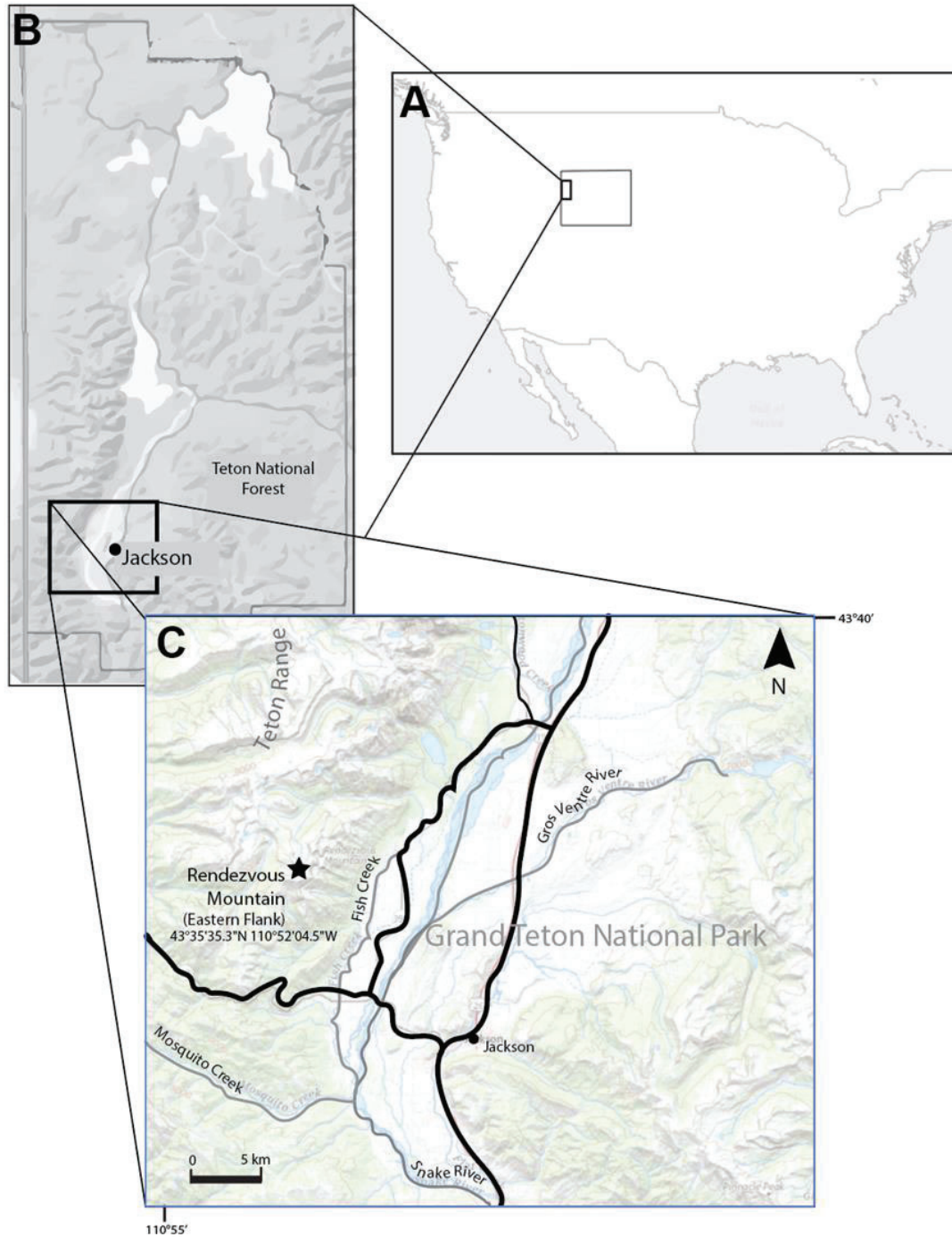


Figure 2. *Location of Rendezvous Mountain section.* (A) Map of the United State denoting the state of Wyoming. (B) Topographic map of western Wyoming. (C) The star denotes the area of study on the eastern flank of the Teton Range.



Figure 3. *Field photo of site.* The Middle Cambrian Gros Ventre and the Upper Cambrian Gallatin Formations of Rendezvous Mountain. The cliff face of the measured section is indicated by the black arrow.

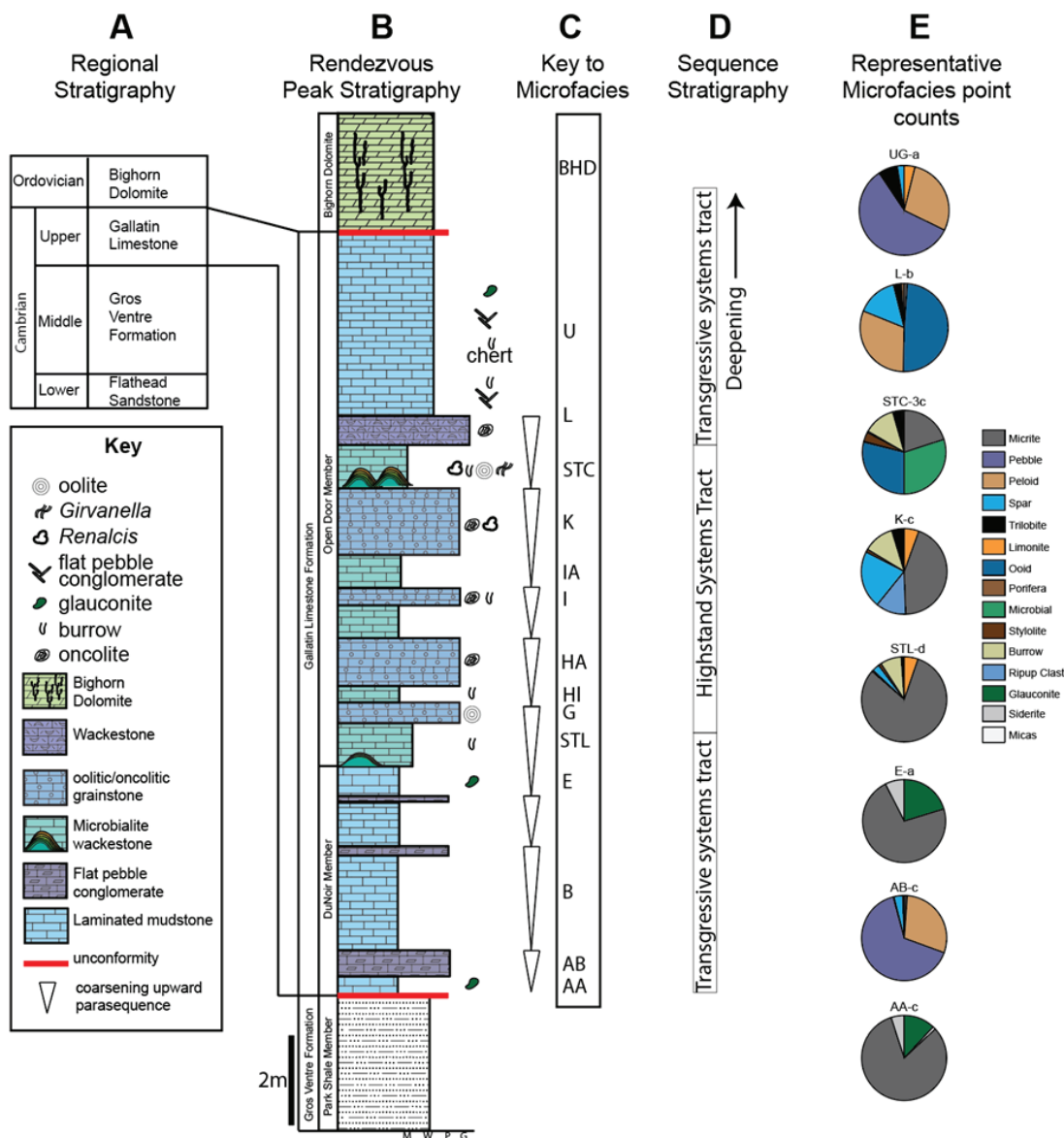


Figure 4. *Stratigraphic, lithologic, and petrographic summary of the study.* (A) Regional stratigraphy of the study area. (B) Stratigraphy of the measured section at Rendezvous Peak. (C) Key to microfacies analyses correlated with the stratigraphy. (D) Interpretation of the sequence stratigraphy. (E) Representative microfacies of the thin section point counts (300 points per slide).

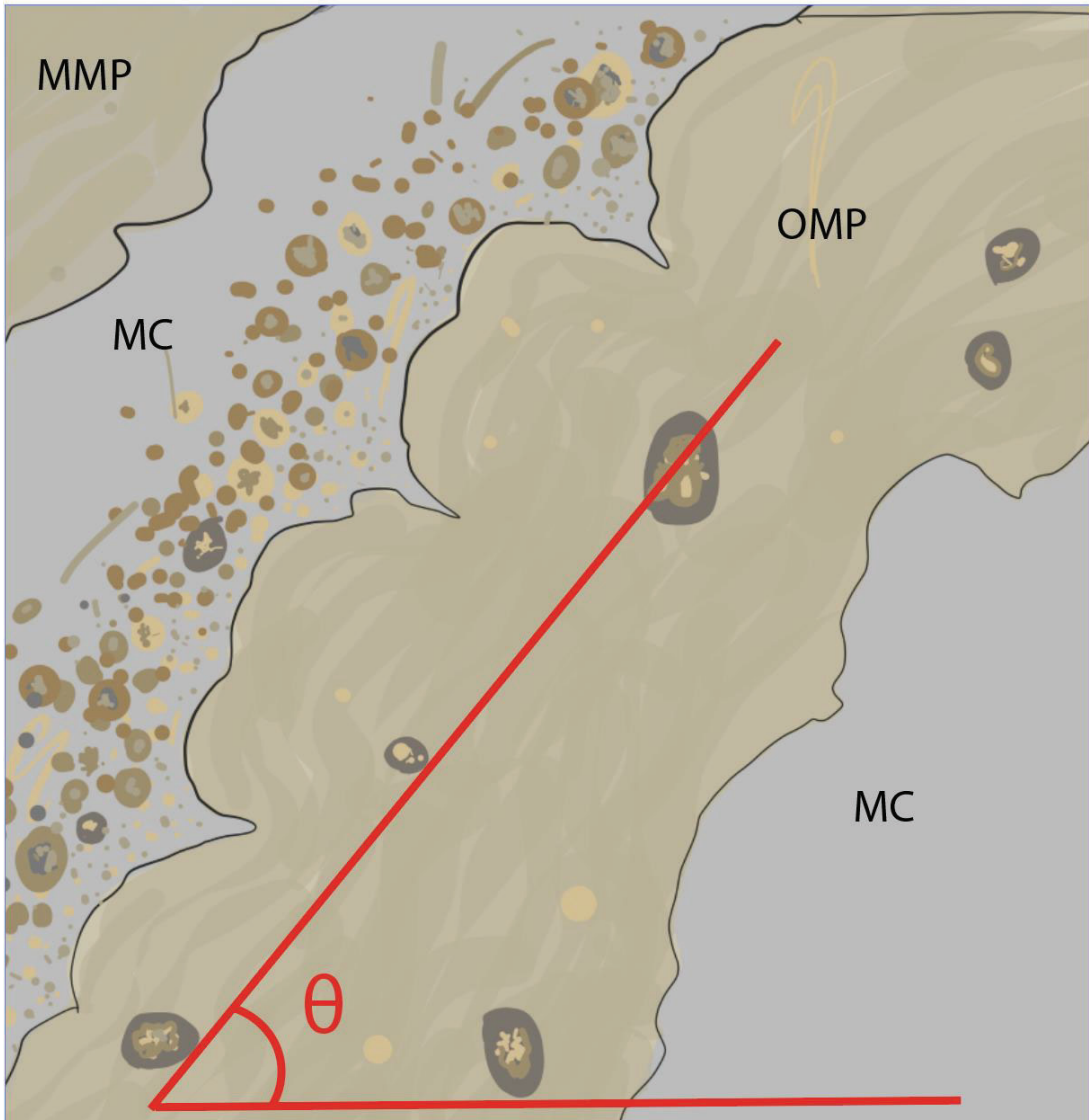


Figure 5. ***Ooid grain diameter-angle height comparison.*** Vertical angle measurements ( $\theta$ ) are used to determine the height of lamination and ooid grains within micrite (*MC*) are measured if found within proximity to or that run parallel to ooid-rich microbial precipitate (*OMP*) lamination.

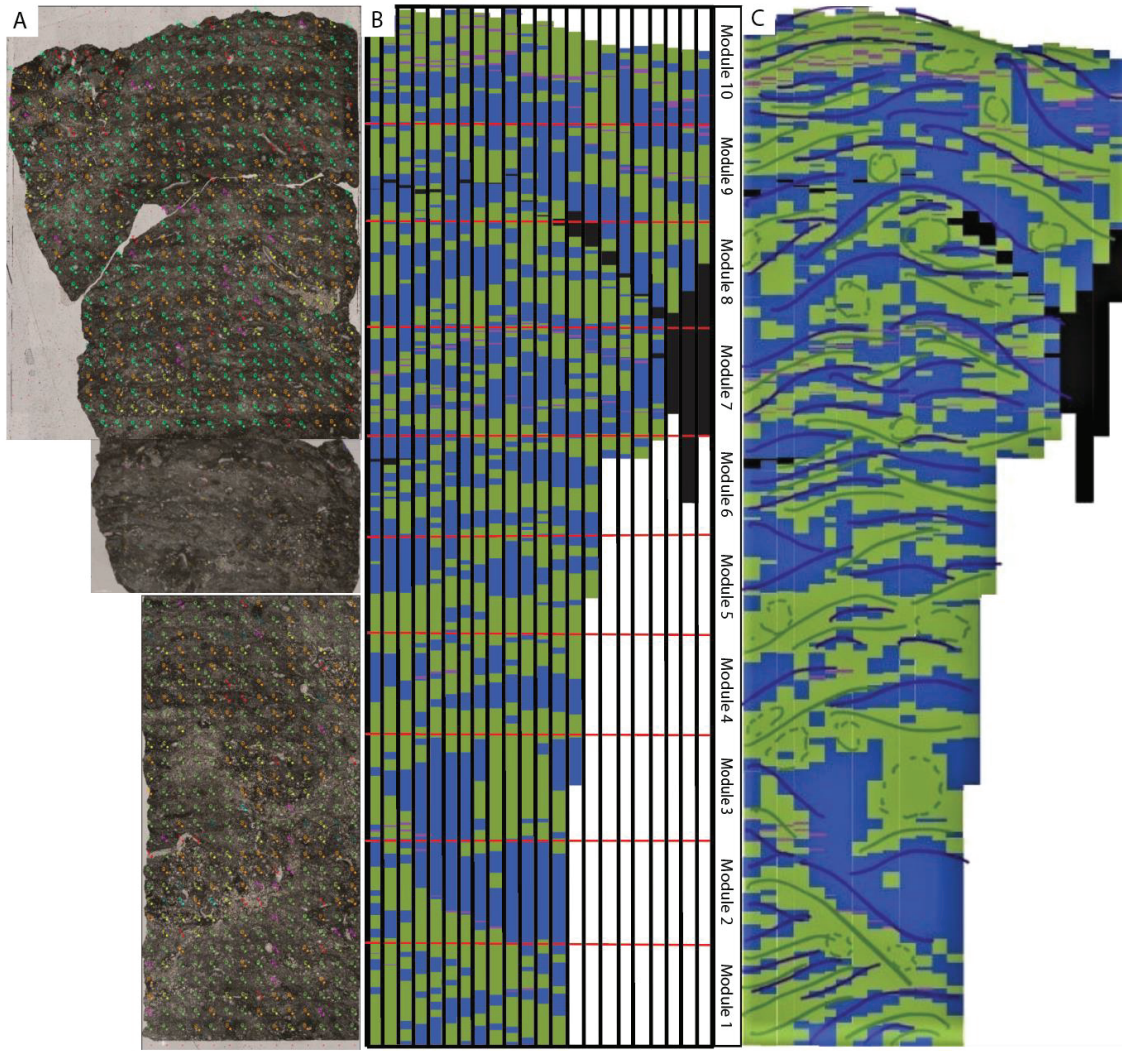


Figure 6. *CMS analysis of STC 1*. (A) Thin section photomicrographs denoting point counts. (B) CMS strips run vertically (there are 24 in total) and modules run horizontally. (C) Annotations indicate distinguished laminations of the *lamination exclusion method* which were numerated. CMS provides a visual interpretation that is simplified. The amount of micritic (blue) and microspar (green) are nearly equal.

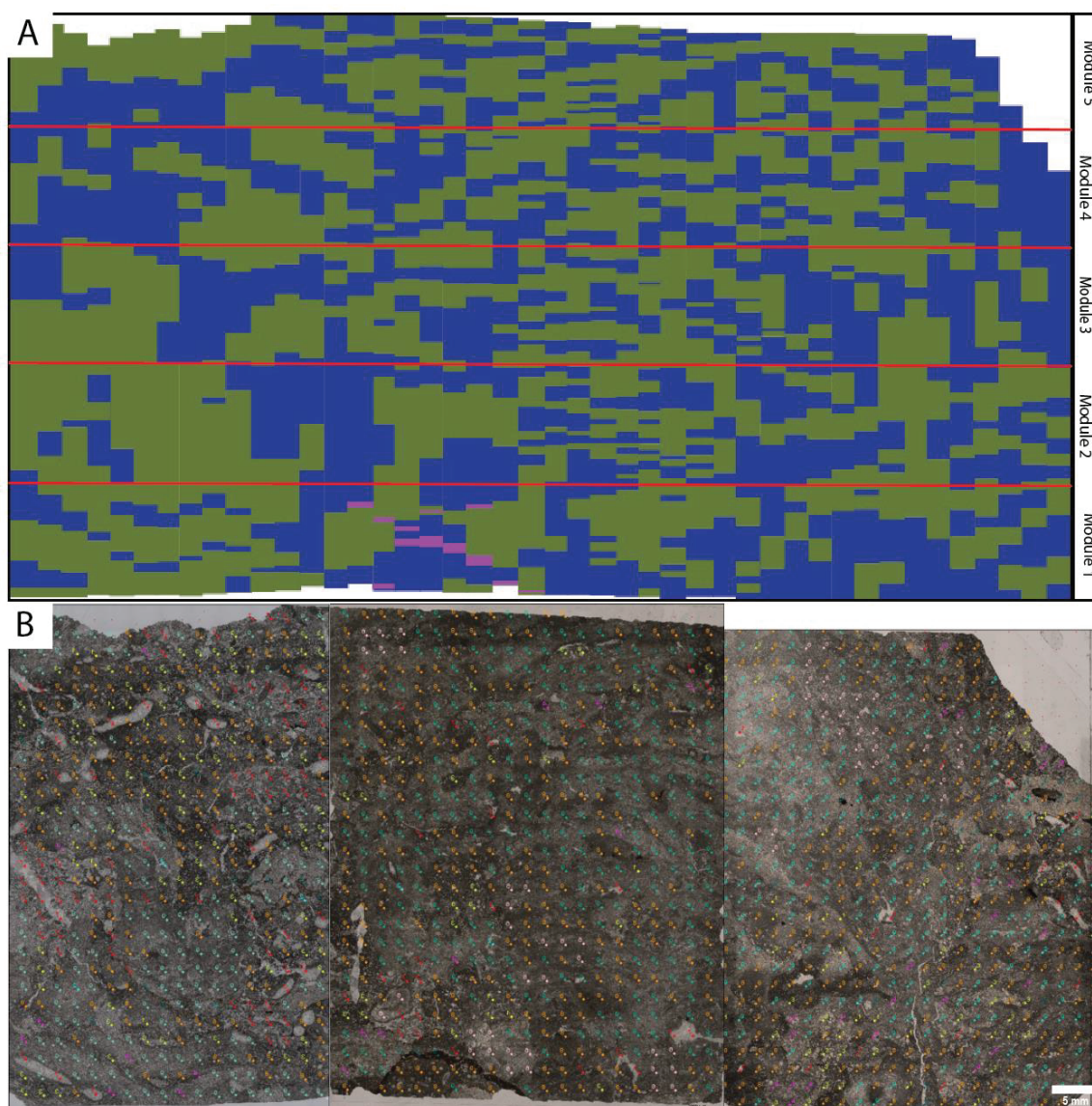


Figure 7. *CMS analysis of STC 2.* (A) CMS of STC2 showing strips running vertically (there are 24 in total) and modules run horizontally. Annotations indicate distinguished laminations of the *lamination exclusion method* which were numerated. The amount of micrite (blue) and microspar (green) frequency bands are equal. (B) Thin section point counts of sample STC 2.



Figure 8. *Stromatolite lenses of the Gallatin Formation*. Basal stromatolitic lenses of the STL layer possess very different microfacies than their upper counterpart. Although the mesostructural surface was only examined in outcrop the absence of vertical growth is notable. Unlike the ooid-bioclast-rich surrounding fill within the STC layer the matrix within STL was carbonate mud with few to no fossils.

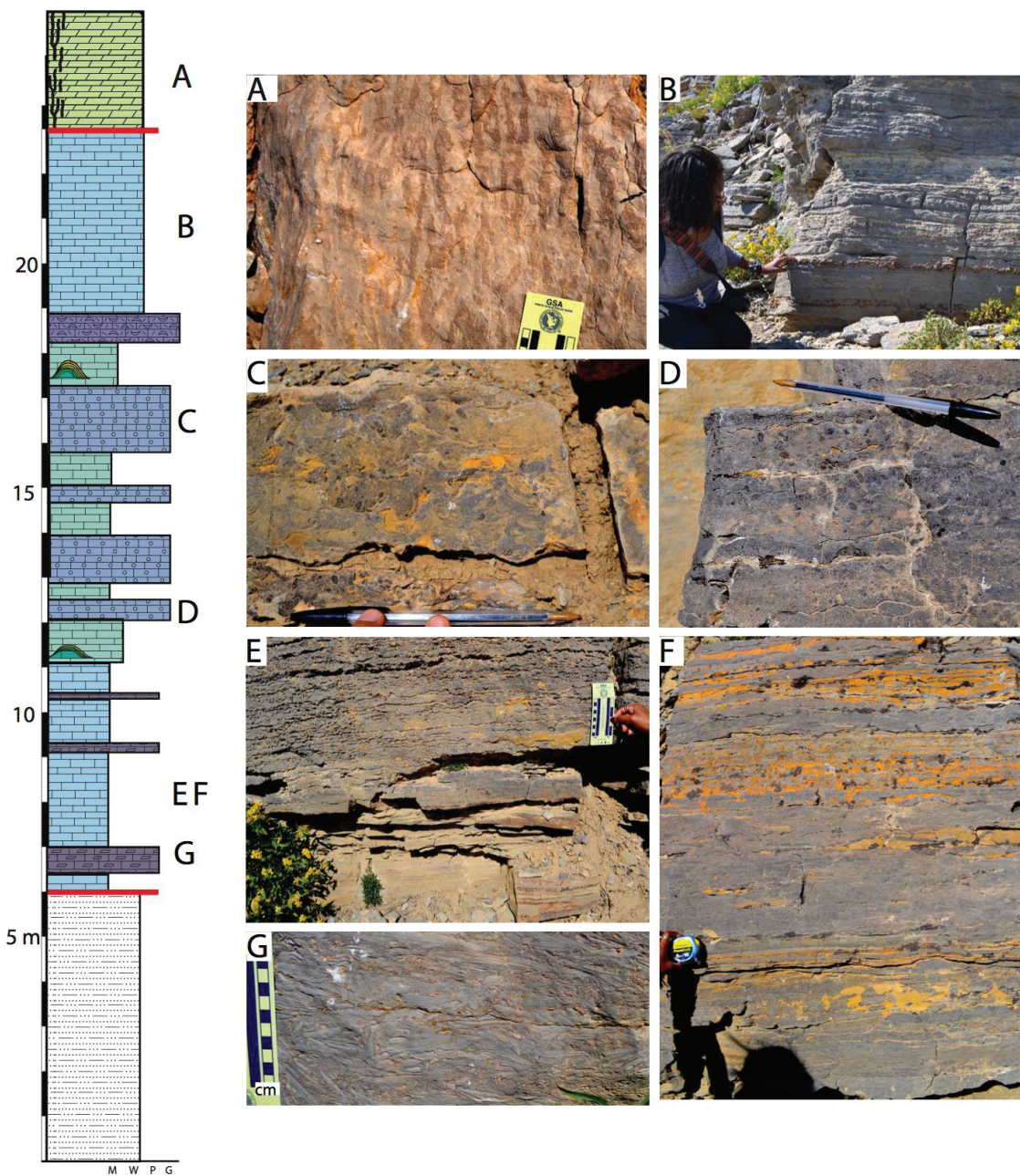


Figure 9. *Representative outcrop photographs and corresponding lithologic section* (see Figure 3 for lithologic key). (A) Mottled fabric of the Bighorn Dolomite. (B) Chert bands in laminated mudstone (Microfacies ‘U’). (C) Oncoid facies denoting U-shaped burrows. (D) Oncoid grainstone facies. (E-F) Laminated mudstone facies (Microfacies ‘AA, B, and E’). (G) Flat pebble conglomerate facies (Microfacies AB).

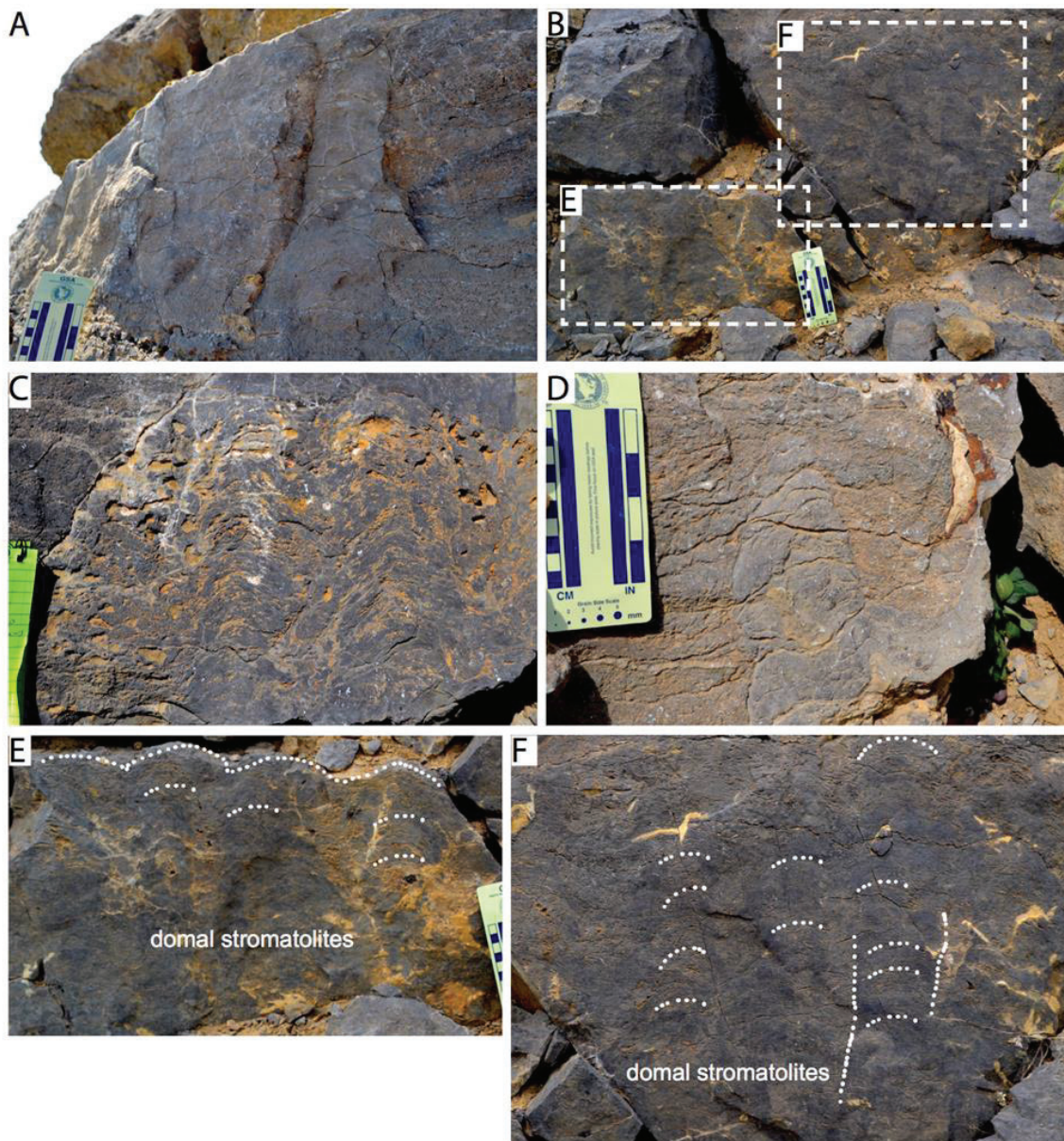


Figure 10. *Outcrop photographs of STC microbialite facies.* (A) Columnar stromatolite surrounded by grainstone fill. (B) Domal stromatolite mounds. (C) Laterally-linked stromatolite facies. (D) Columnar, *Conophyton*-like stromatolite surrounded by grainstone fill. (E-F) Close-up of Figure 5B with annotated lamination and dome morphology.

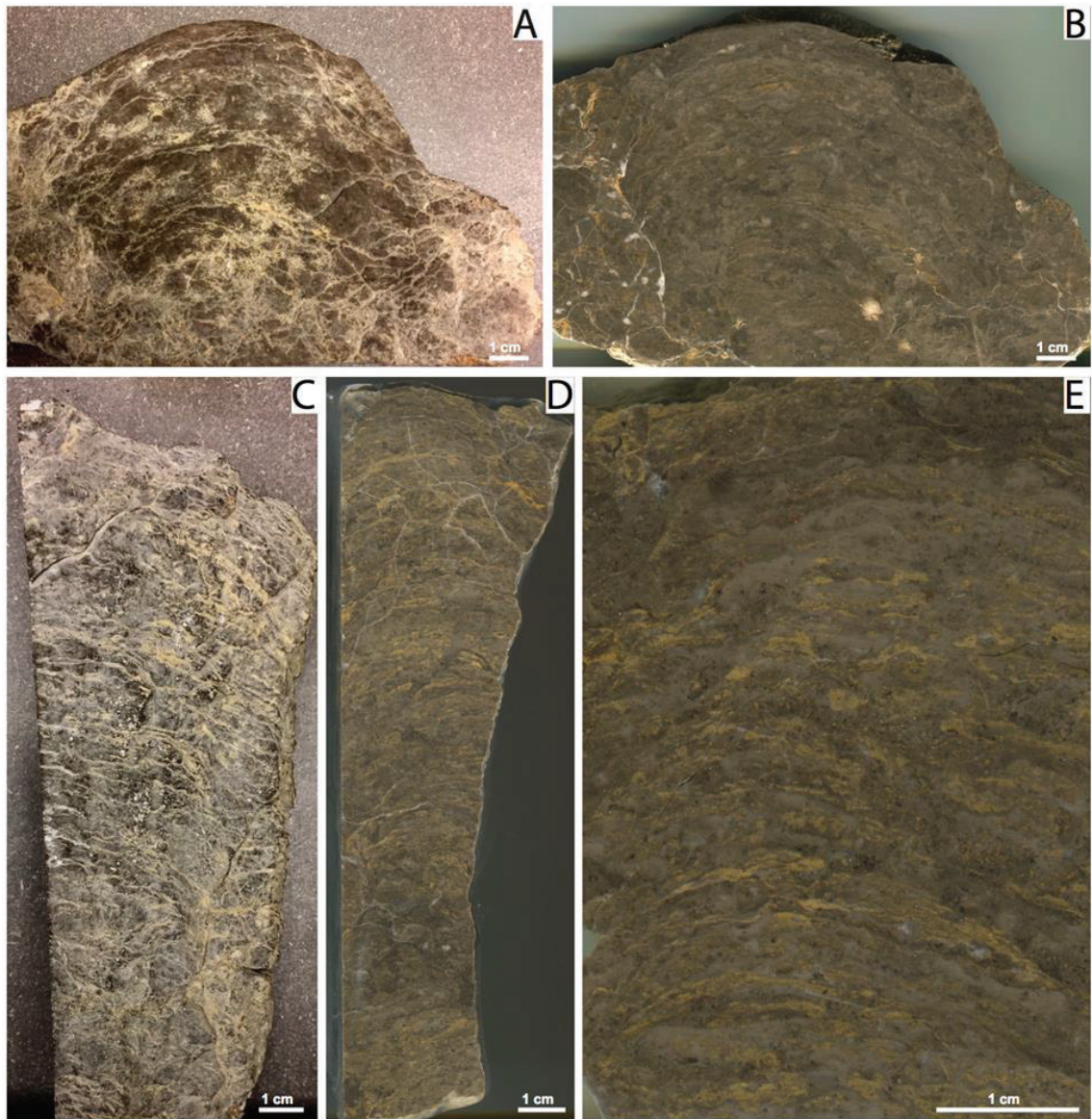


Figure 11. *Mesostructure of STC microbialites*. (A) External texture of sample STC2 showing poorly defined lamination. (B) Polished scan of STC2. (C). External texture of sample STC1. (C-D) Polished scans of STC1. (E) Polished scan of STC1.

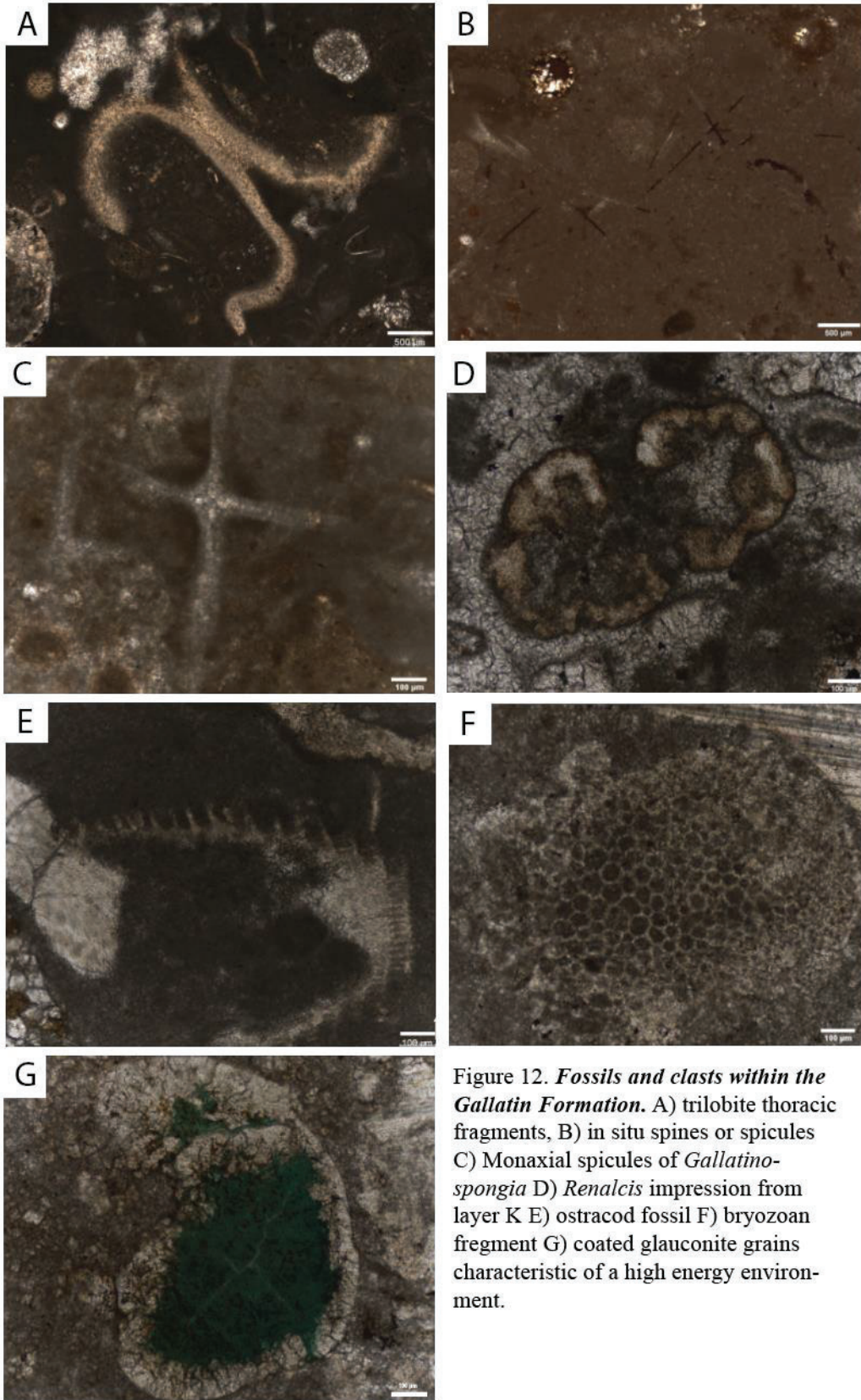


Figure 12. *Fossils and clasts within the Gallatin Formation.* A) trilobite thoracic fragments, B) in situ spines or spicules C) Monaxial spicules of *Gallatinspongia* D) *Renalcis* impression from layer K E) ostracod fossil F) bryozoan fragment G) coated glauconite grains characteristic of a high energy environment.

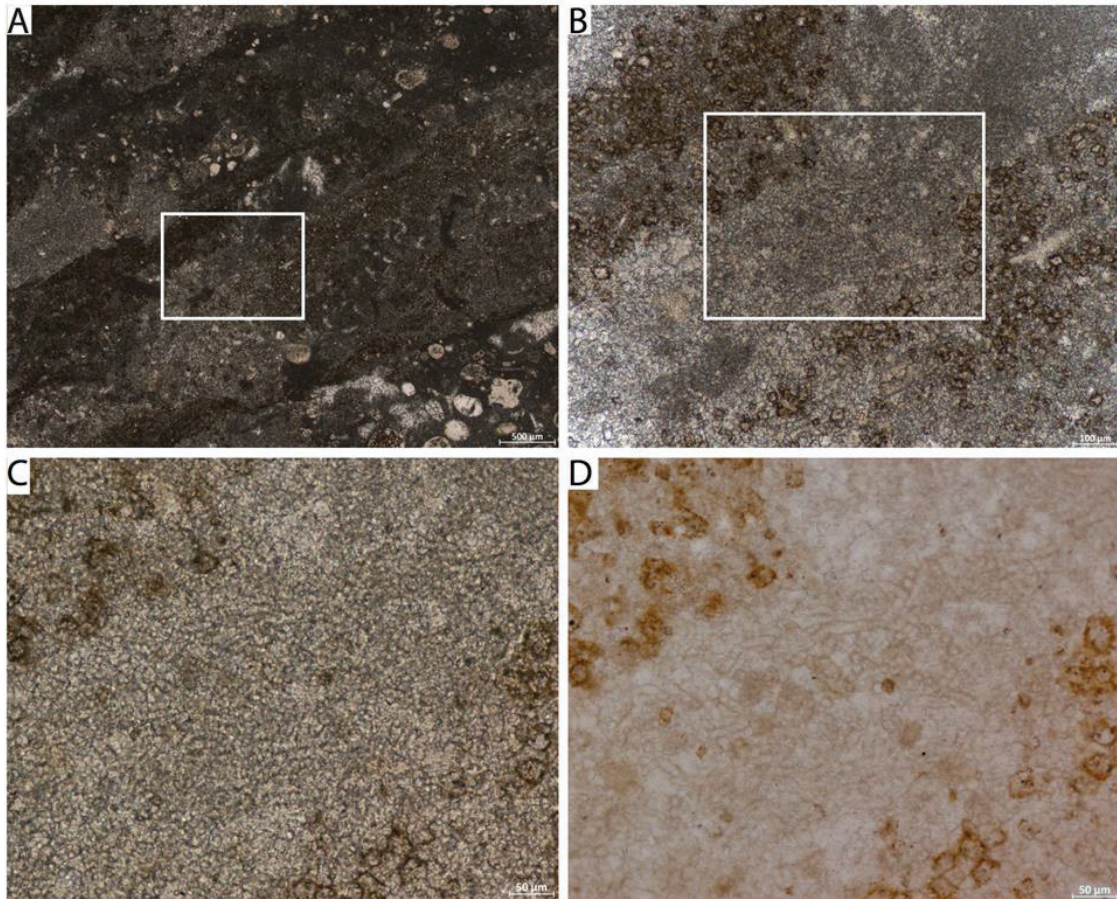


Figure 13. *Microstructure of microbialite sample STC1.* (A) Alternating coarse and fine-grained microsparitic laminae. (B) Close up of square in Figure 7A. (C) Close-up of Figure 7B using plane polarized light. (D) Same field of view as Figure 7C using a white card, the image shows lamination composed of *Girvanella* filaments.

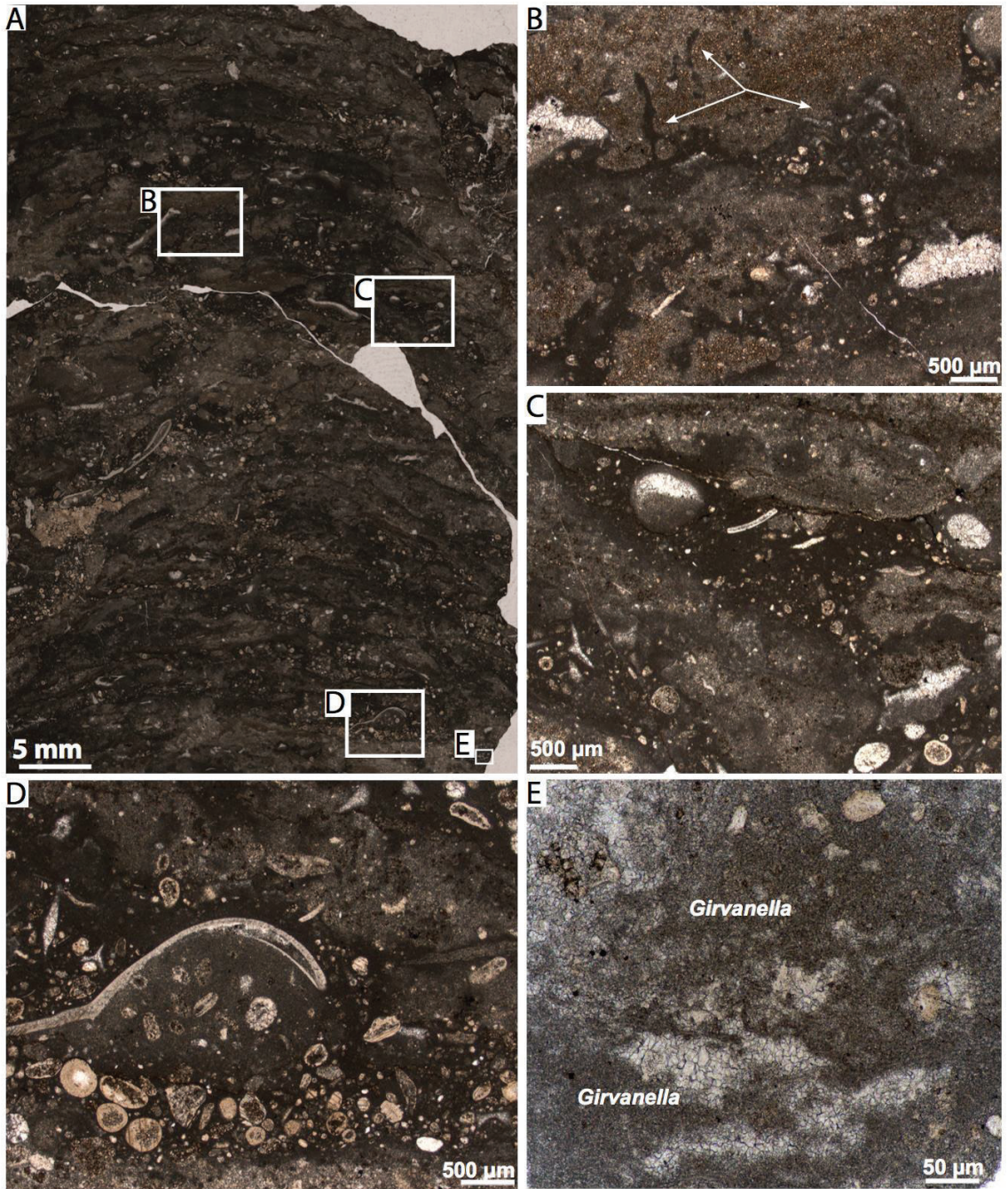


Figure 14. *Microstructure of microbialite sample STC1.* (A) Alternating micritic and sparitic laminae. (B) Micritic, dendritic features (arrows) alternate with microspar layers. (C) Spar-occluded fenestrae. (D-E) Example skeletal, ooid clasts, and *Girvanella* microfossils.

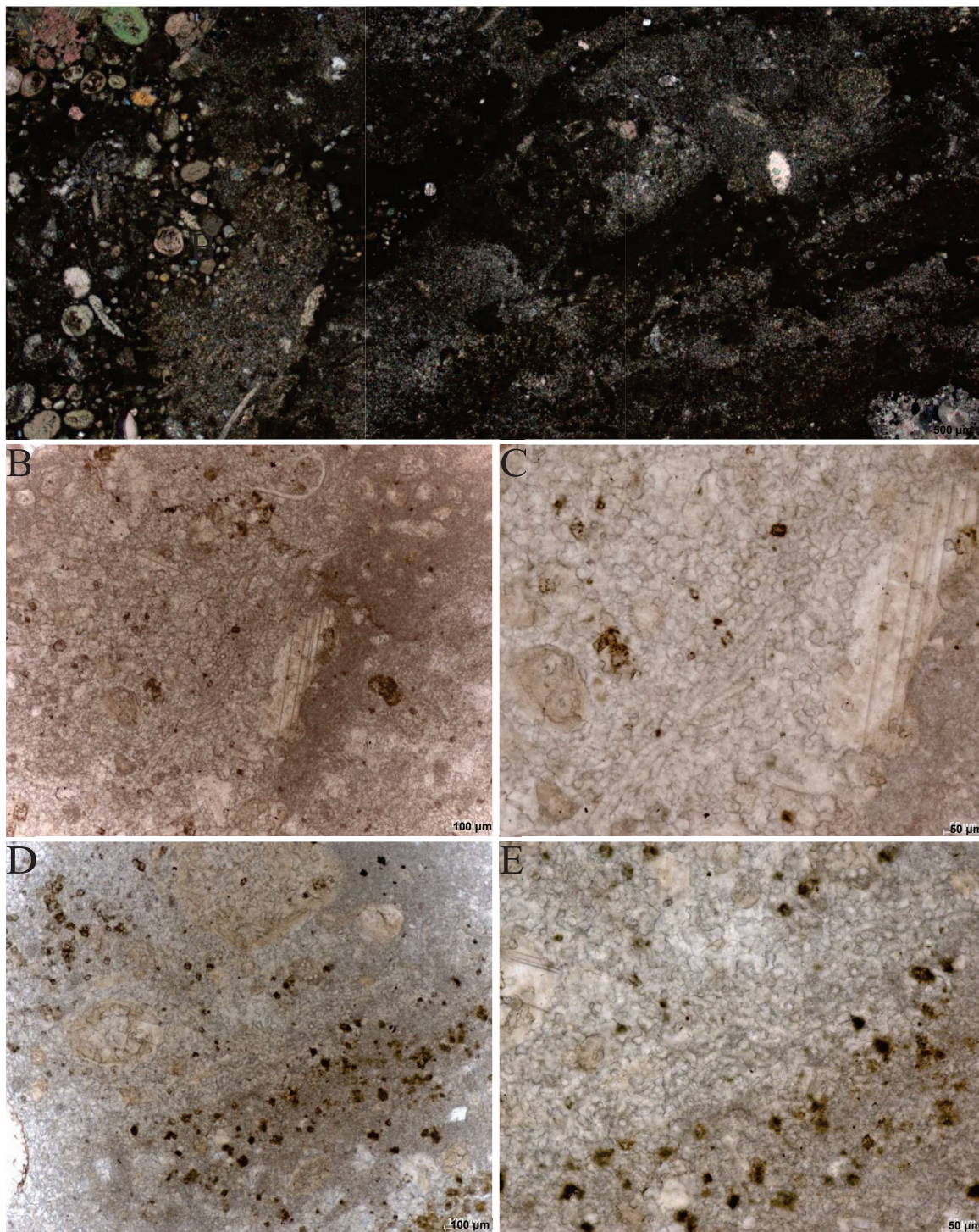


Figure 15. *Microstructure of microbialite sample STC1.* A. Alternating micrite and spar laminae shown in cross polarized light. (B-C) Close up of Figure 7A denoting allochthonous clasts embedded in micrite at a high angle, the outer portion of the grain is encrusted by the microfossil *Girvanella* (images taken using a white card). (D-E) Close up of Figure 7A denoting clasts embedded on *Girvanella* filaments (images taken using a white card).

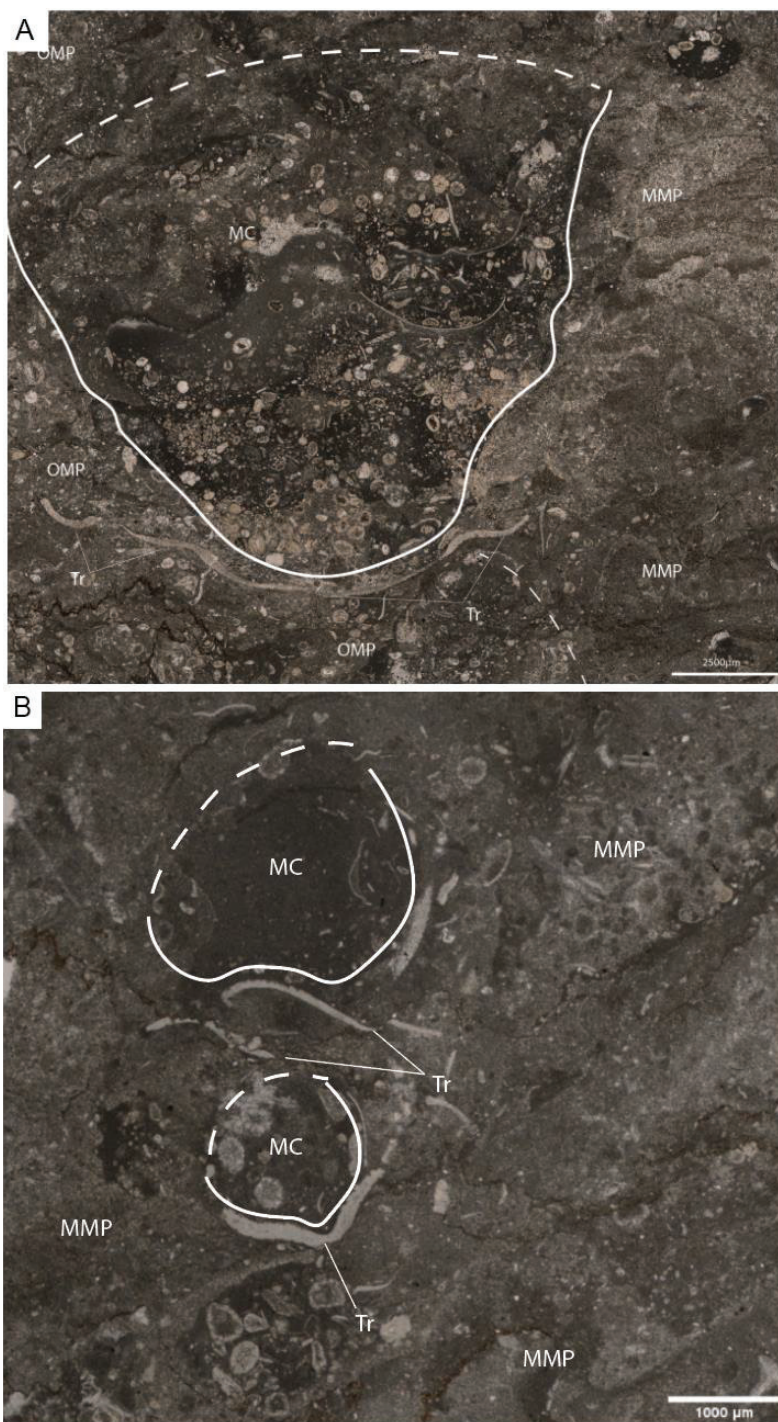


Figure 16. *Truncation of microbially precipitated microspar (MMP) fabric.* The obstruction of calcimicrobial growth by laterally deposited elongate trilobite (*Tr*) fossils is notable where (A) a complete thoracic segment causes microspar (*MMP*) and ooid-rich microspar precipitate (*OMP*) to diverge with compliments to the shape of the fragment (taken from STC 1) which then allows micritic (*MC*) deposits and (B) additional obstructions by trilobite fragments.

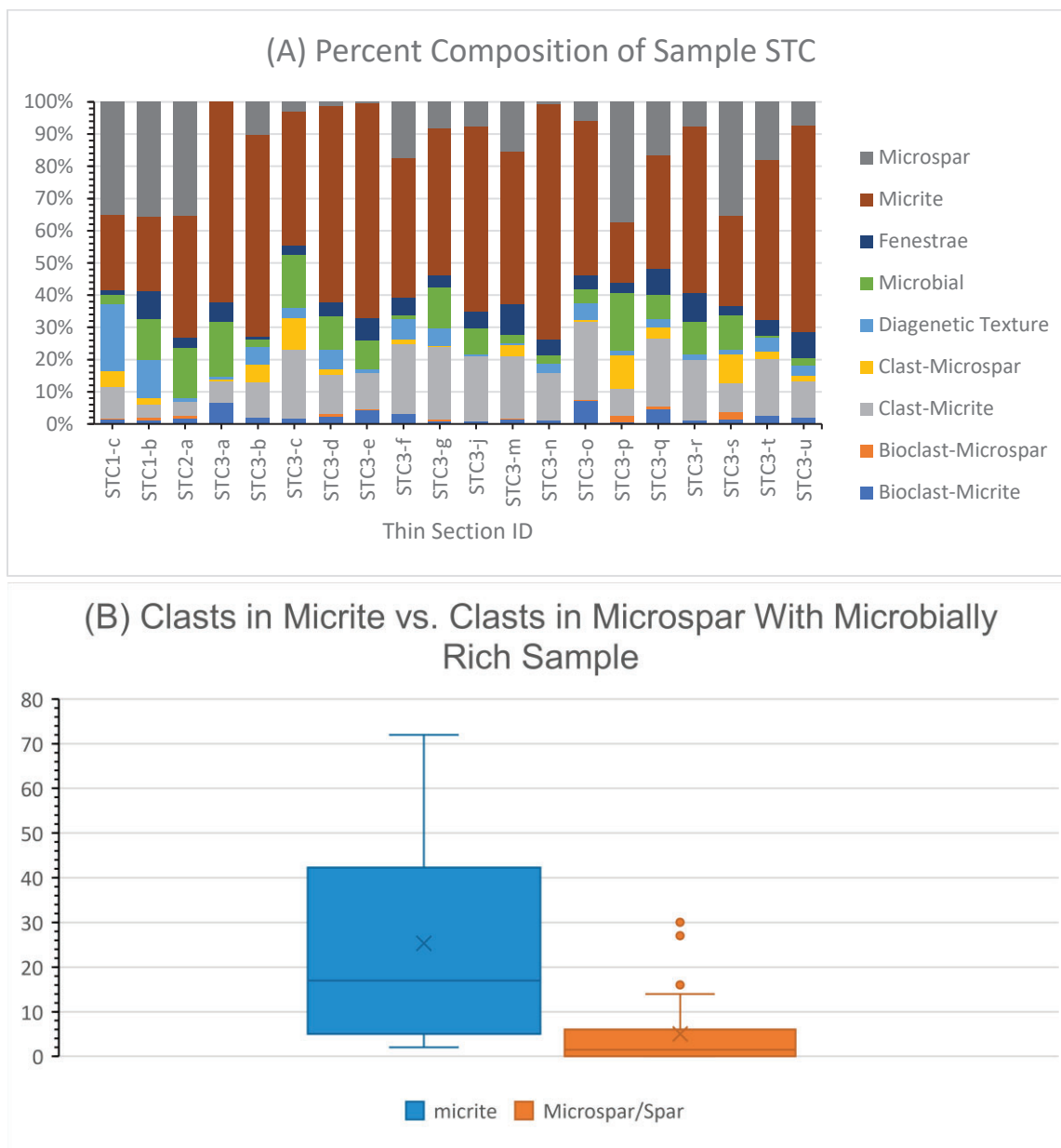


Figure 17. *Point count data of STC microbialites expressed through stacked columns and box plots.* (A) Within the sample layer there is notable variability between microfacies, textures, and allochems. (B) The variability between allochem population of both microfacies and the intense disparity in the average number of allochems within them.

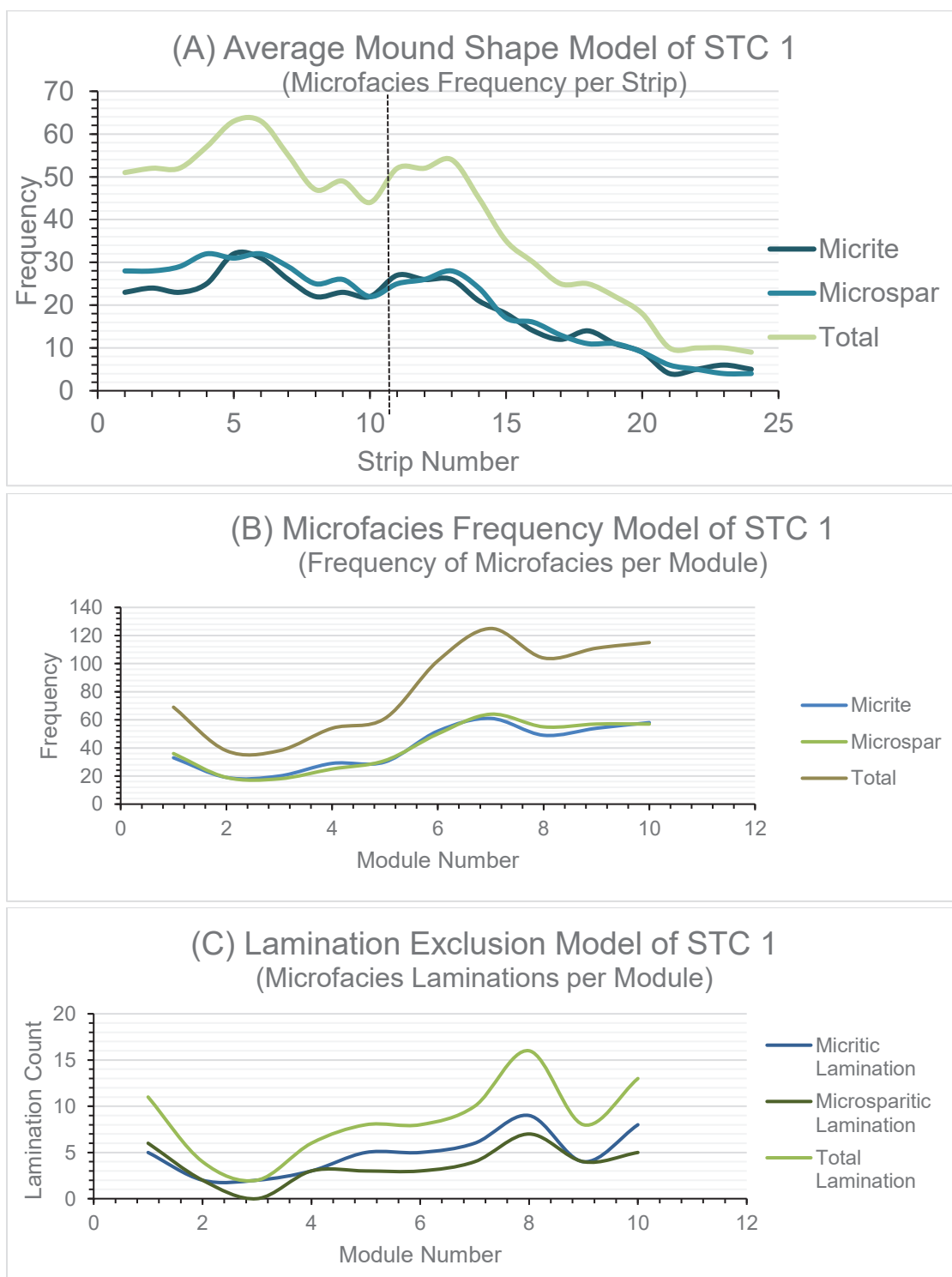


Figure 18. *Microfacies frequency models*. A. Scatter-line graphs displaying the trend of microfacies frequency across the column (strips) and up the column (modules). (B) Microfacies frequency model of STC 1 showing frequency of microfacies per module. (C) Lamination exclusion model.

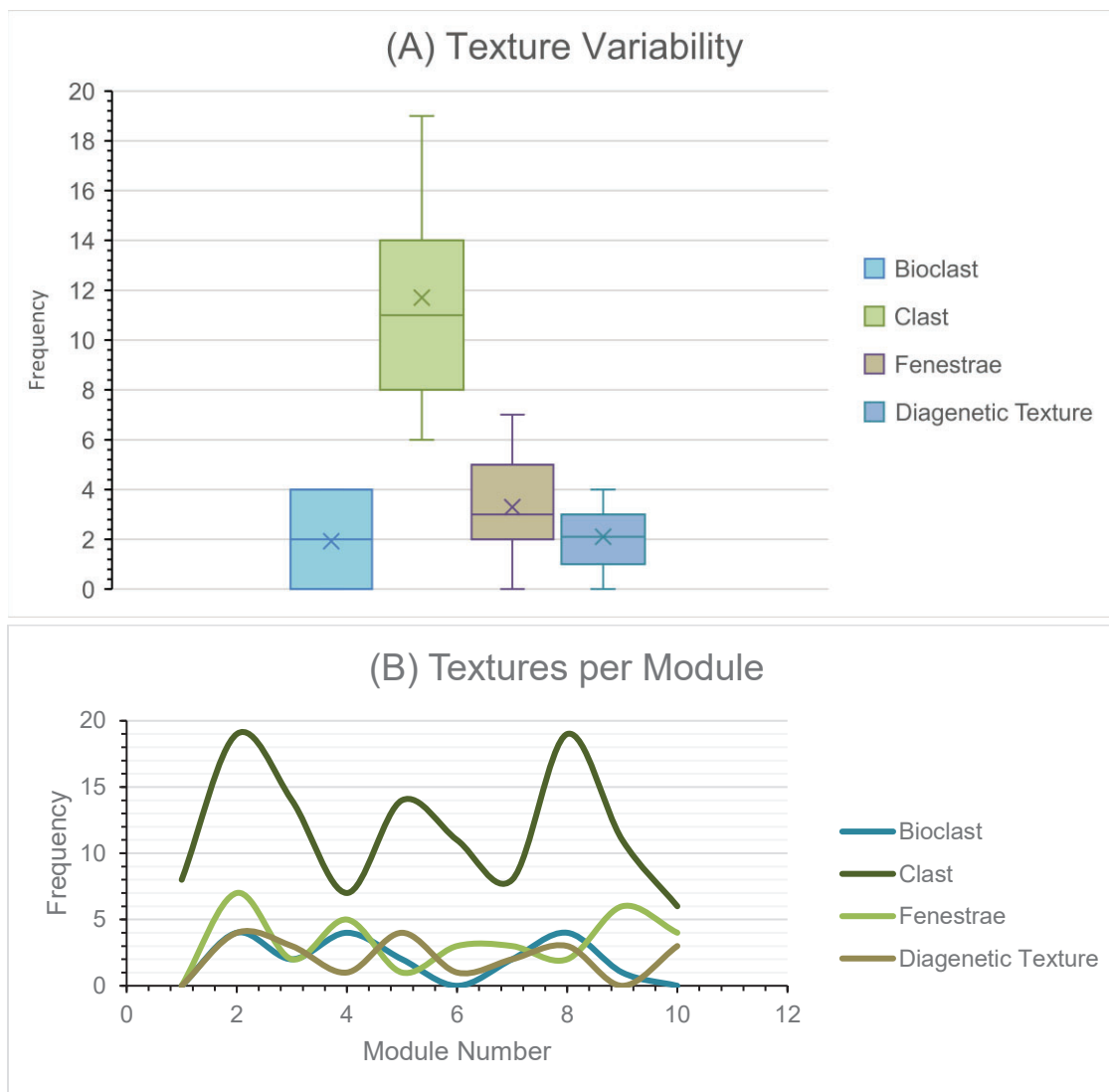


Figure 19. *Texture variability in STC 1.* (A) the variability of textures found within STC 1 and (B) the change in textural frequencies per module. Clast population is notably greater than any other category.

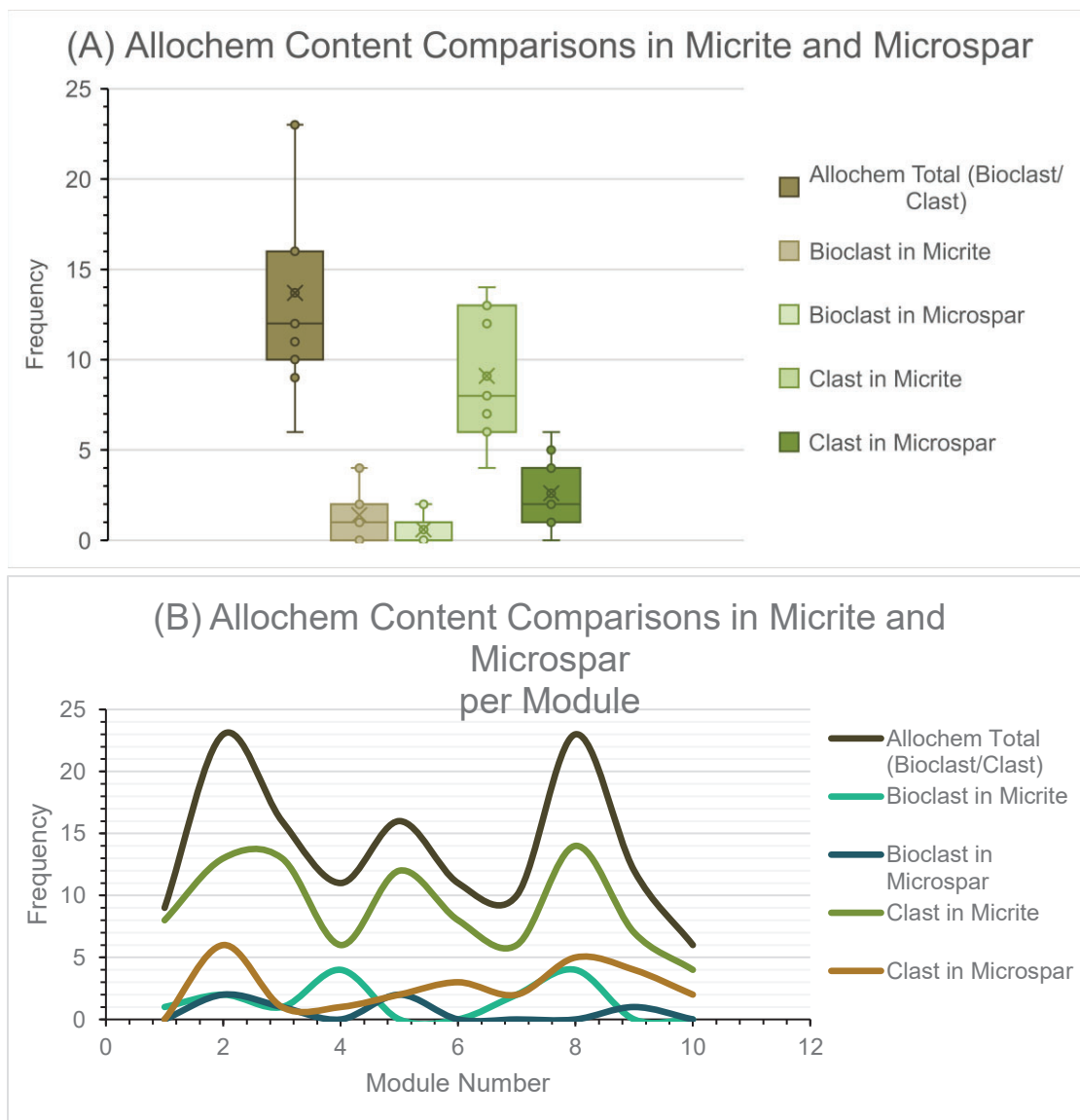


Figure 20. *The variability of allochem content in STC 1.* (A) Box plot displaying the range of each allochem type in each microfacies type and (B) the shift in the frequencies of allochem content per module.

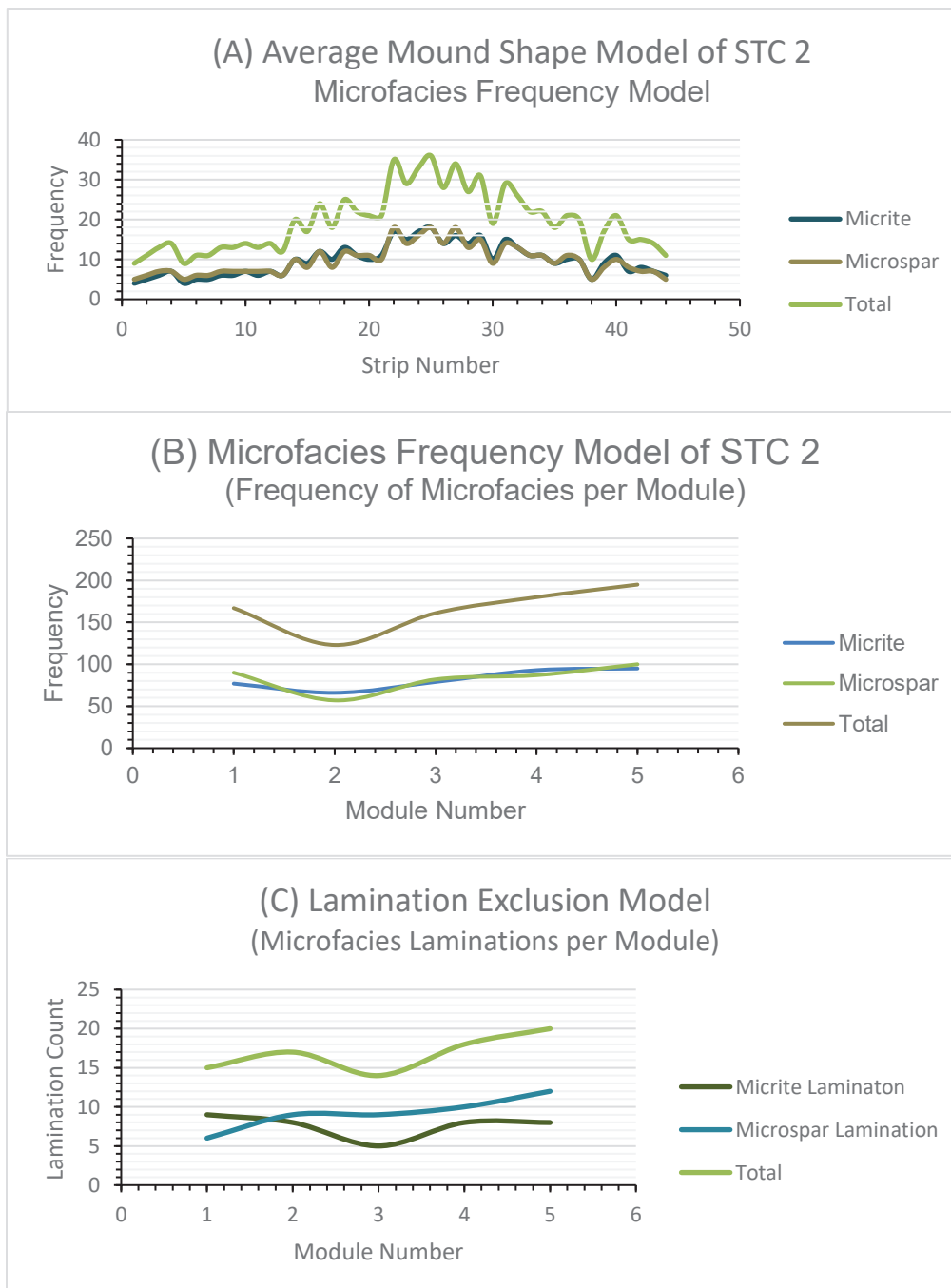


Figure 21. *Microfacies frequency models of STC 2.* (A-C) Scatter-line graphs displaying the trend of microfacies frequency across the column (strips) and up the column (modules). The parabolic shape of the sample is the most characteristic of typical stromatolites.

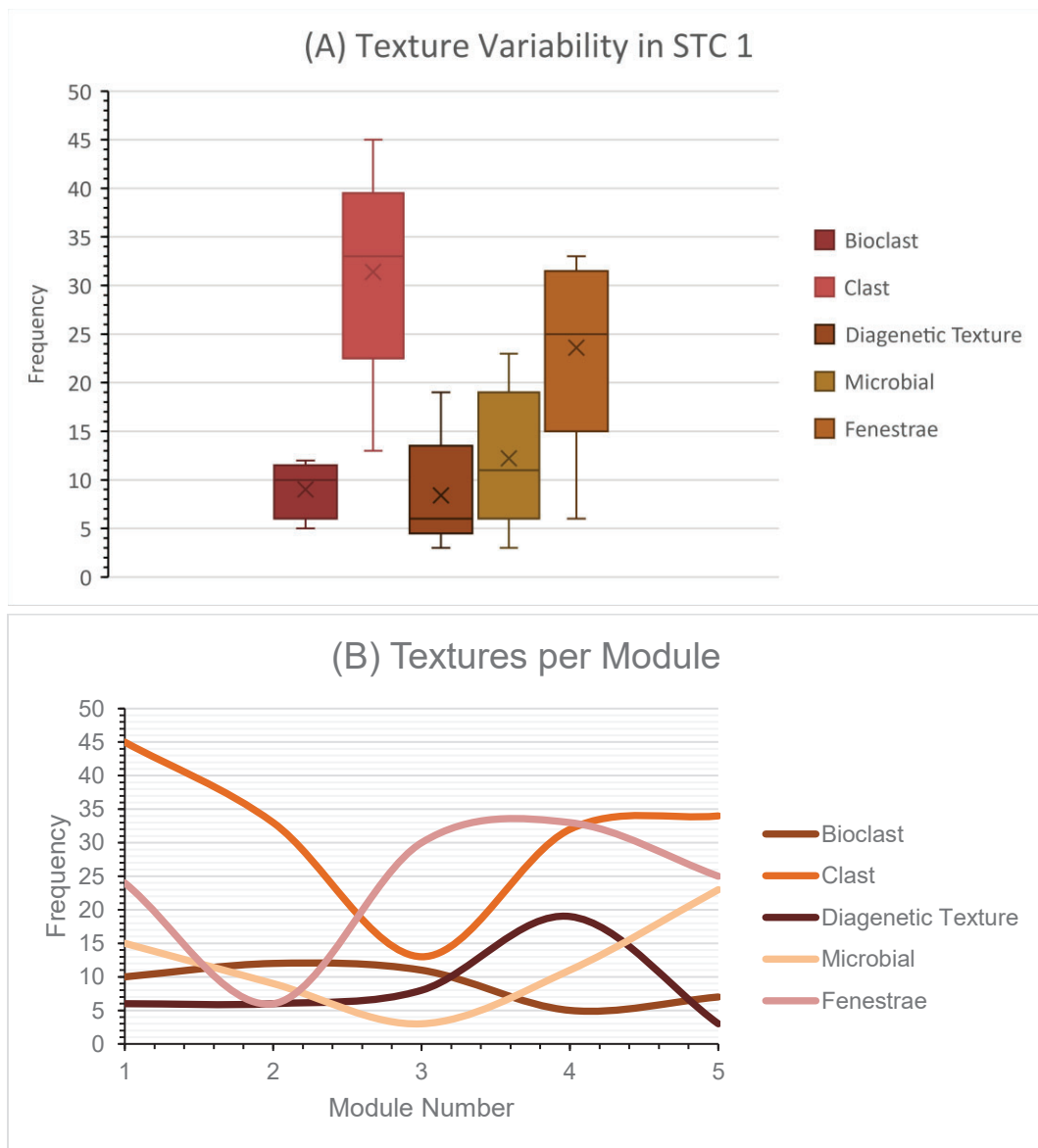


Figure 22. *Texture variability in STC 2.* (A) The variability of textures found within STC 2 and (B) the fluctuation in textural frequencies per module.

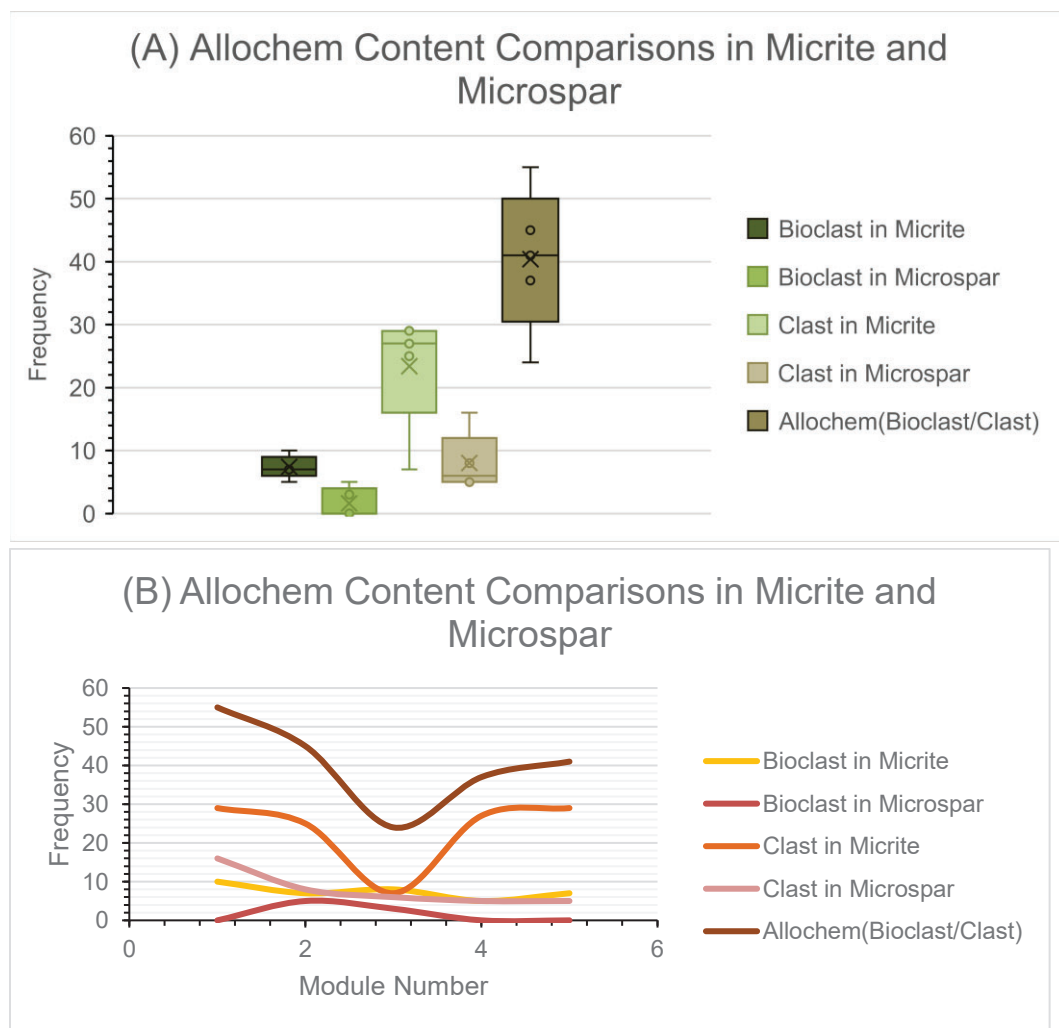


Figure 23. *The variability of allochem content in STC 1.* (A) Box plot displaying the range of each allochem type in each microfacies type and (B) the shift in the frequencies of allochem content through each module.

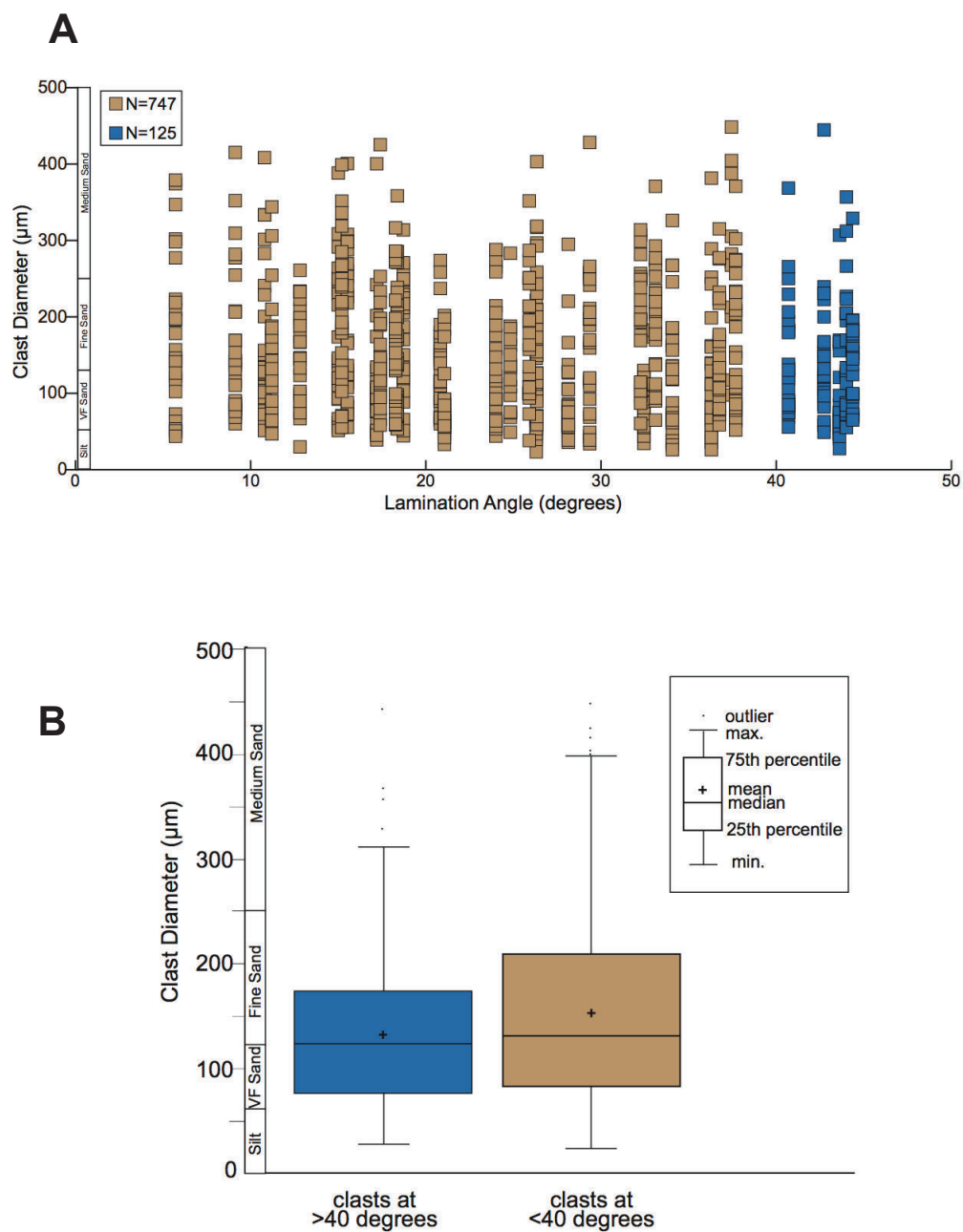


Figure 24. *Relationship between clast (oid) size and lamination angle in the STC (microbialite) layer.* (A) Clast size versus lamination angle. (B) Box and whisker plot of clast diameter showing that there is no statistically significant difference between the size of clasts at >40 degrees and the clasts at <40 degree.

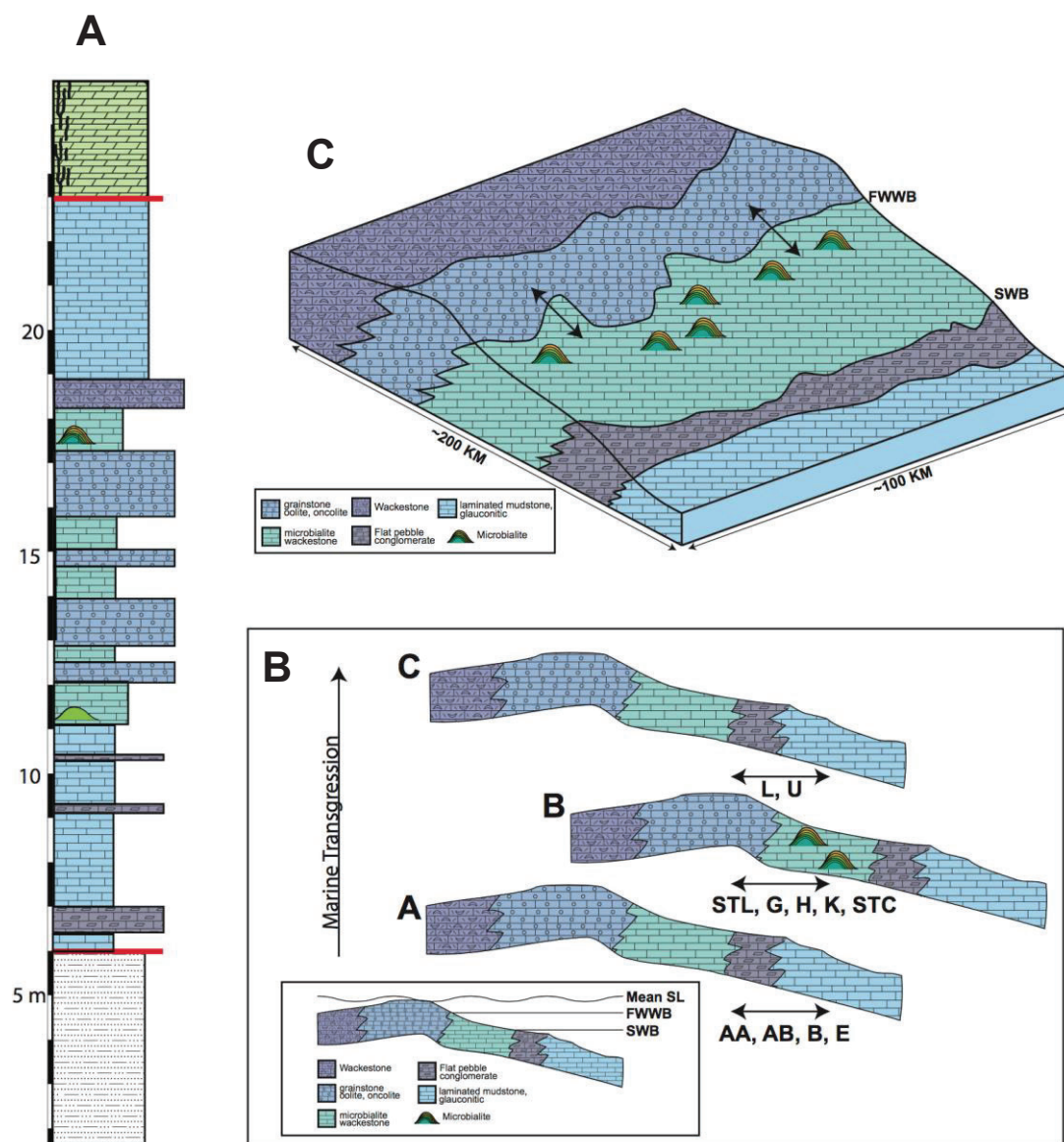


Figure 25. *Stratigraphic column and depositional model of Rendezvous section.* (A) Stratigraphic column of the Gallatin Formation. (B) Stepwise depositional model of the alternating facies types and their associated microfacies. (C) Depositional model interpretation of the STL microbialites next to ooid shoal facies.

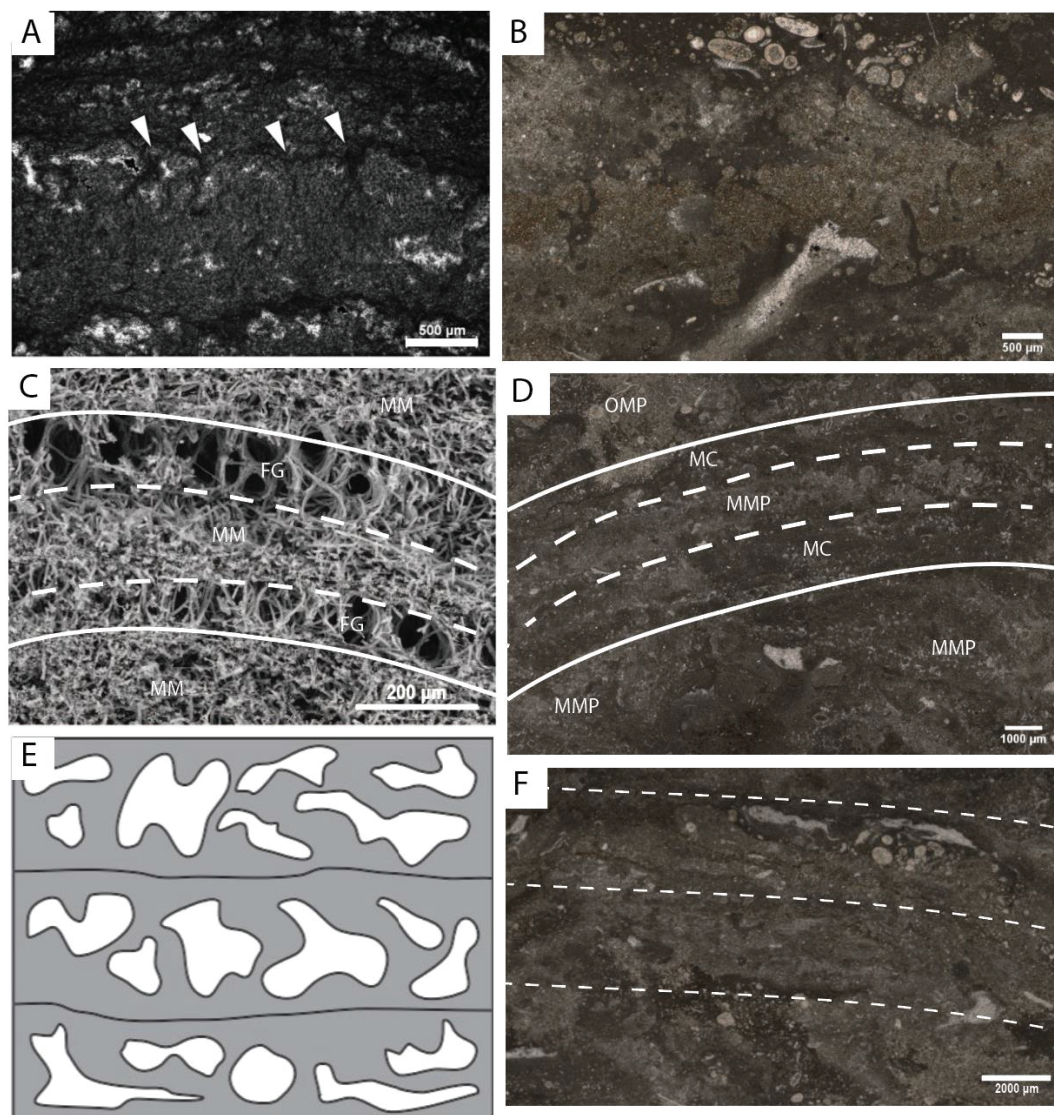


Figure 26. *Textural similarities found in modern and ancient microbialites.* (A) from the Neoproterozoic: partial hourglass structures formed by gas pockets are (B) similar to features in STC 1 but may be of different origin. (C) Caverns between densely filamentous mats are nearly 1:1, analogous to (D) STC 2 where micritic areas are sandwiched between microspar lamina, all of which are of similar width and have a 1:1 ratio of both microfacies according to CMS. (E) Descriptive illustration of irregular occluded fenestrae within areas between mats known to form as a result of metabolic processes. (F) Similar textures occur within STC 2 and are found predominately in micritic facies. (Images A, C, and E from Mata et al., 2012).

## TABLES

Table 1. Point count data displayed as percentages for Gallatin formation samples excluding layer STC.										
Sample ID	Glauconite	imonite	Mica	Bio/Micrite	Microbial	Ooid	Pelsparite	Pelmirite	Peloid	Pebble
AA-b	9%	—	1%	86%	—	—	—	—	—	—
AA-c	12%	—	1%	82%	—	—	—	—	—	—
AB-a	1%	—	—	23%	—	—	—	—	22%	48%
AB-c	—	—	—	1%	—	—	—	—	29%	65%
B-a	—	13%	—	71%	—	—	—	—	—	—
B-d	—	19%	—	74%	—	—	—	—	—	—
E-a	20%	—	—	72%	—	—	—	—	—	—
STL-b	—	9%	—	78%	—	—	—	—	—	—
STL-c	—	6%	—	81%	—	—	—	—	—	—
STL-d	—	5%	—	81%	—	—	—	—	—	—
STL-e	—	8%	—	79%	—	—	—	—	—	—
G-a	—	—	—	4%	—	11%	—	—	—	—
G-d	—	—	—	5%	—	13%	—	—	—	—
H-a	—	12%	—	69%	—	—	—	—	—	—
H-b	—	5%	—	74%	—	—	—	—	—	—
HA-b	—	1%	—	13%	—	—	—	—	5%	—
HA-c	—	—	—	27%	—	—	—	—	20%	—
K-a	—	—	—	37%	—	—	—	—	—	—
K-b	—	12%	—	27%	—	—	—	—	—	—
K-c	—	6%	—	44%	—	—	—	—	—	—
L-a	—	—	—	34%	—	38%	—	—	22%	—
L-b	—	—	—	1%	—	49%	—	—	31%	—
UG-a	—	4%	—	—	—	—	—	—	28%	58%
UG-d	—	1%	—	5%	—	—	41%	—	—	16%
UG-e	—	1%	—	6%	—	—	45%	—	—	28%
UG-f	—	—	—	68%	—	1%	—	—	—	—
UG-h	—	4%	—	1%	—	—	20%	27%	—	—
UG-m	—	36%	—	23%	—	2%	—	—	2%	2%
UG-o	4%	23%	—	—	—	1%	—	34%	—	—
BHD-2	—	—	—	—	39%	—	—	—	—	—
BHD-3vl	—	—	—	—	24%	—	—	—	—	—
BHD-v2	—	—	—	—	17%	—	—	—	—	—
BHD-v4	—	—	—	—	25%	—	—	—	—	—

Table 1 (Continued)										
Clast	Ripup Clast	Siderite	Sparite	Stylolite	Bivalve	Burrow	Trilobite	Porifera	Fossil	Non- Fossil
—	—	4%	—	—	—	—	—	—	—	100%
—	—	5%	—	—	—	—	—	—	—	100%
—	—	1%	4%	—	—	1%	—	—	1%	99%
—	—	—	3%	—	—	—	—	—	—	100%
—	—	1%	—	3%	—	12%	—	—	12%	88%
—	—	—	—	1%	1%	4%	—	—	5%	95%
—	—	7%	—	—	—	—	—	—	—	100%
—	—	—	3%	—	—	4%	4%	2%	9%	91%
—	—	—	3%	2%	—	7%	1%	—	8%	92%
—	—	—	3%	1%	—	8%	1%	—	9%	91%
—	—	—	2%	5%	—	5%	2%	—	7%	93%
27%	14%	—	37%	5%	—	—	1%	—	1%	99%
24%	25%	—	29%	2%	—	—	2%	—	2%	98%
—	—	—	3%	6%	—	10%	—	—	10%	90%
—	—	—	7%	4%	—	8%	—	1%	9%	91%
50%	—	—	18%	3%	1%	6%	5%	—	11%	89%
26%	—	—	5%	2%	1%	16%	3%	—	20%	80%
—	28%	—	12%	5%	—	13%	5%	1%	18%	82%
—	11%	—	39%	3%	1%	1%	6%	—	7%	93%
—	11%	—	22%	1%	—	12%	5%	—	16%	84%
—	—	—	2%	—	—	—	4%	—	5%	95%
—	—	—	15%	—	—	—	3%	1%	4%	96%
—	—	—	7%	—	—	—	2%	—	2%	98%
—	—	—	—	4%	—	24%	8%	—	32%	68%
—	—	—	2%	2%	3%	9%	4%	—	17%	83%
—	—	—	2%	—	—	25%	5%	—	29%	71%
—	—	—	—	3%	—	44%	1%	—	45%	55%
—	—	2%	—	1%	7%	1%	24%	—	32%	68%
—	—	1%	—	—	15%	—	20%	2%	37%	63%
—	—	—	60%	—	—	—	1%	—	1%	99%
—	—	—	76%	—	—	—	—	—	—	100%
—	—	—	83%	—	—	—	—	—	—	100%
—	—	—	74%	1%	—	—	—	—	—	100%

Table 2. Point count data from layer STC (sample STC1-3) representing 300 points per sample.

Sample ID	Bioclast in Micrite	Bioclast in Microspar	Clast in Micrite	Clast in Microspar	Diagenetic Texture	Microbial	Fenestrae	Micrite	Microspar	Total
STC1-c	1%	0%	10%	5%	21%	3%	2%	23%	35%	100%
STC1-b	1%	1%	4%	2%	12%	13%	9%	23%	36%	100%
STC2-a	2%	1%	4%	0%	1%	16%	3%	38%	35%	100%
STC3-a	7%	0%	7%	1%	1%	17%	6%	62%	0%	100%
STC3-b	2%	0%	11%	5%	6%	2%	1%	63%	10%	100%
STC3-c	2%	0%	21%	10%	3%	17%	3%	41%	3%	100%
STC3-d	2%	1%	12%	2%	6%	11%	4%	61%	1%	100%
STC3-e	4%	0%	11%	0%	1%	9%	7%	67%	0%	100%
STC3-f	3%	0%	22%	2%	6%	1%	6%	43%	17%	100%
STC3-g	1%	0%	23%	0%	5%	13%	4%	45%	8%	100%
STC3-j	1%	0%	20%	0%	1%	8%	5%	57%	8%	100%
STC3-m	1%	0%	19%	4%	0%	3%	10%	47%	15%	100%
STC3-n	1%	0%	15%	0%	3%	3%	5%	73%	1%	100%
STC3-o	7%	0%	24%	1%	5%	5%	4%	48%	6%	100%
STC3-p	1%	2%	8%	10%	2%	18%	3%	19%	37%	100%
STC3-q	5%	1%	21%	3%	3%	7%	8%	35%	17%	100%
STC3-r	1%	0%	19%	0%	2%	10%	9%	52%	8%	100%
STC3-s	1%	2%	9%	9%	1%	11%	3%	28%	35%	100%
STC3-t	3%	0%	18%	2%	5%	0%	5%	50%	18%	100%
STC3-u	2%	0%	11%	2%	3%	2%	8%	64%	7%	100%

Table 3A. STC 1 Microfacies Correlation Data							
Spearman's $\rho$		Fenestrae	Diagenetic Texture	Bioclast in Micrite/Microspar	Clast in Micrite/Microspar	Allochem in Micrite	
<b>Micrite Frequency</b>	Correlation Coefficient	.012	-.390	-.328	-.606**	-.328	
	Level of Significance	.487	.132	.177	.032	.177	
<b>Microspar Frequency</b>	Correlation Coefficient	.080	-.351	-.497*	.222	-.497*	
	Level of Significance	.414	.160	.072	.269	.072	
Table 3B. STC 2 Microfacies Correlation Data							
Spearman's $\rho$		Diagenetic Texture	Microbial	Fenestrae	Bioclast in Micrite/Microspar	Clast in Micrite/Microspar	Allochem in Micrite
<b>Micrite Frequency</b>	Correlation Coefficient	-.051	.500	.700*	-.410	.359	-.410
	Level of Significance	.467	.196	.094	.246	.276	.246
<b>Microspar Frequency</b>	Correlation Coefficient	-.462	.900*	.200	-.894**	-.308	-.894**
	Level of Significance	.217	.019	.374	.020	.307	.020
*. Correlation is significant at the 0.10 level (1-tailed).							
**. Correlation is significant at the 0.05 level (1-tailed).							
***. Correlation is significant at the 0.01 level (1-tailed).							

Table 4. Average ooid diameter to lamina angle height		
Angle ID	Degree	Average Ooid/Clast ( $\mu\text{m}$ )
1	37.4	272.4
2	24.8	133.4
3	37.7	164.4
4	28.1	92.6
5	36.3	120.8
6	20.8	137.8
7	17.2	111.8
8	15.0	165.1
9	5.7	176.5
10	9.1	161.5
11	18.7	173.8
12	18.4	148.9
13	26.3	106.6
14	29.4	165.9
15	34.1	129.9
16	26.3	183.5
17	24.0	142.3
18	17.4	156.0
19	15.5	185.3
20	36.8	154.9
21	43.6	89.1
22	18.3	160.0
23	15.2	206.4
24	32.4	93.6
25	10.8	165.5
26	12.8	152.4
27	44.0	147.5
28	33.1	192.3
29	42.7	145.1
30	21.1	87.6
31	11.2	142.7
32	32.3	188.0
33	40.7	143.8
34	25.9	166.1
35	44.4	141.4

## APPENDICIES

Strip Number	Micrite	Microspar	Total
1	4	5	9
2	5	6	11
3	6	7	13
4	7	7	14
5	4	5	9
6	5	6	11
7	5	6	11
8	6	7	13
9	6	7	13
10	7	7	14
11	6	7	13
12	7	7	14
13	6	6	12
14	10	10	20
15	9	8	17
16	12	12	24
17	10	8	18
18	13	12	25
19	11	11	22
20	10	11	21
21	11	10	21
22	17	18	35
23	15	14	29
24	17	16	33
25	18	18	36
26	14	14	28
27	16	18	34
28	14	13	27
29	16	15	31
30	10	9	19
31	15	14	29
32	13	13	26
33	11	11	22
34	11	11	22
35	9	9	18
36	10	11	21
37	10	10	20
38	5	5	10
39	9	8	17
40	11	10	21
41	7	8	15
42	8	7	15
43	7	7	14
44	6	5	11
Total	429	429	858

Appendix 1. *Raw data of STC 1 microfacies frequency per strip*

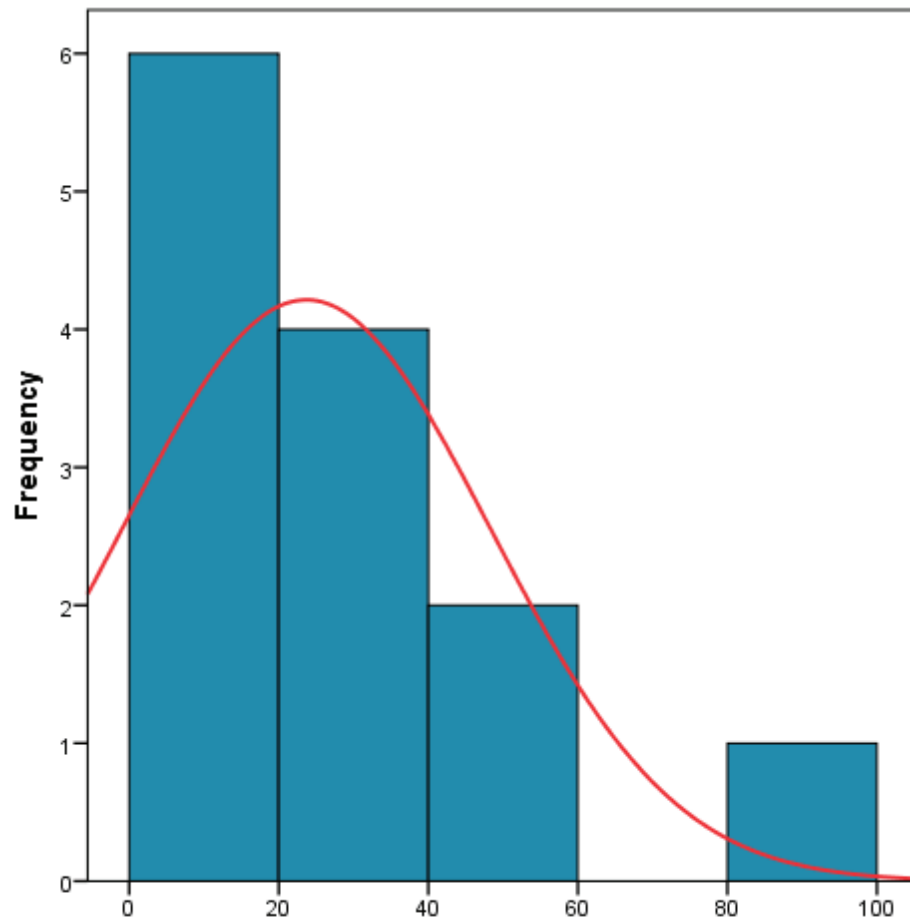
Appendix 2. Raw data of STC 1 microfacies and texture frequency per module.										
Module Number	1	2	3	4	5	6	7	8	9	10
Microfacies Frequency										
Micrite	33	19	20	29	30	52	61	49	54	58
Microspar	36	19	18	25	31	50	64	55	57	57
Total	69	38	38	54	61	102	125	104	111	115
Lamination Count										
Micritic Lamination	5	2	2	3	5	5	6	9	4	8
Microsparitic Lamination	6	2	0	3	3	3	4	7	4	5
Total Lamination	11	4	2	6	8	8	10	16	8	13
Texture Frequency										
Bioclast		4	2	4	2	0	2	4	1	0
Clast	8	19	14	7	14	11	8	19	11	6
Fenestrae	0	7	2	5	1	3	3	2	6	4
Diagenetic Texture	0	4	3	1	4	1	2	3	0	3
Allochem Frequency										
Bioclast in Micrite	1	2	1	4	0	0	2	4	0	0
Bioclast in Microspar	0	2	1	0	2	0	0	0	1	0
Clast in Micrite	8	13	13	6	12	8	6	14	7	4
Clast in Microspar	0	6	1	1	2	3	2	5	4	2

Appendix 3. Raw data of STC 2 microfacies frequency per strip.				
Strip Number	Micrite	Microspar	Total	
1	23	28	51	
2	24	28	52	
3	23	29	52	
4	25	32	57	
5	32	31	63	
6	31	32	63	
7	26	29	55	
8	22	25	47	
9	23	26	49	
10	22	22	44	
11	27	25	52	
12	26	26	52	
13	26	28	54	
14	21	24	45	
Total	351	385	736	
15	18	17	35	
16	14	16	30	
17	12	13	25	
18	14	11	25	
19	11	11	22	
20	9	9	18	
21	4	6	10	
22	5	5	10	
23	6	4	10	
24	5	4	9	
Total	449	481	930	

Appendix 4. Raw data of STC 2 microfacies and texture frequency per module					
Module	1	2	3	4	5
Microfacies Frequency					
Micrite	77	66	79	93	95
Microspar	90	57	82	87	100
Total	167	123	161	180	195
Lamination Count					
Micrite Laminaton	9	8	5	8	8
Microspar Lamination	6	9	9	10	12
Total	15	17	14	18	20
Texture Frequency					
Bioclast	10	12	11	5	7
Clast	45	33	13	32	34
Diagenetic Texture	6	6	8	19	3
Microbial	15	9	3	11	23
Fenestrae	24	6	30	33	25
Allochem Frequency					
Bioclast in Micrite	10	7	8	5	7
Bioclast in Microspar	0	5	3	0	0
Clast in Micrite	29	25	7	27	29
Clast in Microspar	16	8	6	5	5
Allochem(Bioclast/Clast)	55	45	24	37	41

**(A) Descriptive Statistics of Rendezvous Section**

	Minimum	Maximum	Mean	Std. Deviation
Avg. Fossil Content	0	84	23.69	24.611



**(B) Average Fossil Content of Rendezvous Section**

Appendix 5. *Descriptive statistic and histogram of the average fossil content of Rendezvous section.* Averages calculated from the amount of fossil content to represent the thirteen layers they were collected from.